

Federal Aviation Administration

DOT/FAA/AM-21/26
Office of Aerospace Medicine
Washington, DC 20591

Human Bronchial Epithelial Cells Display Alterations in Chromatin Accessibility and Gene Expression According to Oxygen Availability

Scott J. Nicholson[1], David C. Hutchings[2], Jordan P. Metcalf[3]

[1]FAA Civil Aerospace Medical Institute, 6500 S. MacArthur Blvd Rm. 354, Oklahoma City, OK 73125
[2]Venesco, LLC, 14801 Murdock Street Suite 125, Chantilly, VA 20151
[3]University of Oklahoma Health Sciences Center, 1100 N Lindsay, Oklahoma City, OK 73104

March 2021

NOTICE

This document is disseminated under the sponsorship of the U.S. Department of Transportation in the interest of information exchange. The United States Government assumes no liability for the contents thereof.

_____

This publication and all Office of Aerospace Medicine technical reports are available in full-text from the Civil Aerospace Medical Institute's publications Web site:
www.faa.gov/go/oamtechreports

Technical Report Documentation Page

1. Report No.	2. Government Accession No.	3. Recipient's Catalog No.
DOT/FAA/AM-21/26		

4. Title and Subtitle	5. Report Date
Human Bronchial Epithelial Cells Display Alterations in Chromatin Accessibility and Gene Expression According to Oxygen Availability	March 2021
	6. Performing Organization Code

7. Author(s)	8. Performing Organization Report No.
Scott J. Nicholson[1], David C. Hutchings[2], Jordan P. Metcalf[3]	

9. Performing Organization Name and Address	10. Work Unit No. (TRAIS)
[1]FAA Civil Aerospace Medical Institute, 6500 S. MacArthur Blvd Rm. 354, Oklahoma City, OK 73125 [2]Venesco, LLC, 14801 Murdock Street Suite 125, Chantilly, VA 20151 [3] University of Oklahoma Health Sciences Center, 1100 N Lindsay, Oklahoma City, OK 73104	11. Contract or Grant No.

12. Sponsoring Agency name and Address	13. Type of Report and Period Covered
Office of Aerospace Medicine Federal Aviation Administration 800 Independence Ave., S.W. Washington, DC 20591	14. Sponsoring Agency Code AAM-1

15. Supplemental Notes

CAMI Aerospace Medical Research Division Project No. 2014-AAM-612-GEN-10091

16. Abstract

Aircraft passengers and crew experience mild hypoxia during flight equivalent to an 8,000-ft elevation. Hypoxia is known to induce physiological and transcriptional changes that function together to permit normal cellular and tissue function at reduced oxygen (O_2) levels. Short-term physiological responses include increased respiration and mild tachycardia; short-term transcriptional responses promote glycolysis and initiate angiogenesis, hematopoiesis, and other mitigating adaptations. Hypoxia also induces changes in nuclear chromatin structure, altering histone methylation and chromatin accessibility profiles to promote or inhibit the transcription of specific genes. We assayed chromatin accessibility and gene expression in human bronchial epithelial cells (HBECs) treated at 21%, 15% (the equivalent of aircraft cabin pressurization), and 2% O_2 (typical of tissue hypoxia). Large-scale changes in chromatin accessibility and gene expression were observed at 15% O_2, including upregulation of histone genes and a reduction in intergenic and intronic chromatin accessibility. The 2% O_2 treatment exhibited fewer changes in relation to the 21% O_2 treatment and were mainly limited to the hypoxic response. *ANGPTL4*, an angiogenic regulator, increased at 2% O_2 but decreased at 15% O_2. Further, downregulation of the master regulator of the hypoxic response, *HIF1α*, was predicted at 15% O_2 based on the expression status of the genes it regulates. In summary, HBECs exposed to 15% O_2 for 16 hours exhibit a large-scale transcriptional and nucleosomal response that appears to exclude most hypoxia regulators and, instead, triggers a response possibly promoting altitude acclimatization.

17. Key Words	18. Distribution Statement
Hypoxia, Gene Expression, RNA microarray, ATAC-seq, Bronchial Epithelium	Document is available to the public through the Internet: http://www.faa.gov/go/oamtechreports/

19. Security Classif. (of this report)	20. Security Classif. (of this page)	21. No. of Pages	22. Price
Unclassified	Unclassified	37	

Acknowledgements

We would like to acknowledge and thank the Federal Aviation Administration and the Civil Aerospace Medical Institute for supporting this research, as well as Vicky White, Susan Muster, Dr. Hilary Uyhelji, Leland Booth, and Dr. Dennis Burian for valuable consultations and advice during the conduct and analysis of this study.

Contents

Introduction 1

Methods 2

Cell culture and treatment 2

ATAC-sequencing 3

Microarray analysis 3

ATAC-seq differential peak analysis 4

Motif analysis 4

Microarray bioinformatics analysis 5

Determining microarray-ATAC peak concordance 5

Results and Discussion 5

ATAC-seq 5

Peak Calling and Differential Peak Expression Analysis Reveal Chromatin Accessibility Differences Between Oxygen Treatments 7

ATAC-seq Signals Display Differences According to Expression 12

Gene Expression Analysis by Microarray 14

Concordance Between Differentially Expressed Genes and Peaks Reveals Upregulation of Histones in 15pct Treatment 16

Pathway Analysis Predicts Downregulation of Proliferative Responses at 15pct O_2 and Upregulation of Hypoxic Response at 2pct O_2 18

Transcription factor motif analysis 24

Conclusions 26

Supplementary Tables 28

References 29

List of Tables and Figures

Figure 1. Crossover study designed to examine differences between smokers and nonsmokers during simulated flight. **3**

Figure 2. Blood oxygen saturation (finger) and exhaled gas measurements (as determined by gas chromatograph) over the course of the ground or flight altitude treatment. **4**

Figure 3. Cell counts and concentrations in cellular lavage samples (BAL cells) and cellular composition of those lavage samples. **9**

Figure 4. Gene expression in cellular populations as a result of condition and treatment. **11**

Table 1. Differential Expression count resulting from comparisons between altitude treatment and smoking status. **12**

Figure 5. Differentially expressed and hypoxia-limited gene lists show distinct gene expression patterns based on smoking status in HBEC and BAL cells. **12**

Figure 6. Venn diagram detailing differential expression similarities between HBEC, BAL, and blood samples. **13**

Table 2. Bars indicate magnitude and direction of differential regulation (log fold-change) of indicated genes in each cell type. **14**

Table 3. Top 5 Differentially Regulated IPA® Canonical Pathways in Smokers vs. Nonsmokers During Flight **16**

Figure 7. Upstream regulator networks in common between BAL and HBEC cells in smokers during flight in IPA®. **17**

Table 4. IPA® Predicted Upstream Regulators Among DE Genes in HBEC and BAL Flight Smokers **18**

Table 5. Identified IPA® Networks Among HBEC and BAL cells. **20**

Figure 8. Top-scoring networks in HBEC and BAL cells display differing transcriptional responses regulating *ERK1/2*. **21**

Table 6. Differential Expression Among Blood Sample Contrasts **22**

Figure 9. Comparison of activation state of diseases and biological function pathways in smokers during flight conditions for HBEC and BAL cells. **23**

Figure 10. Hotelling T^2 score histogram and top transcript cluster for each contrast of blood-derived gene expression values. **24**

Figure 11. Top network identified in FS-FN comparison in blood samples. **26**

Supplementary Tables, Figures, and Files **29**

Introduction

Commercial aviators and frequent flyers spend a large proportion of their time in flight, during which they are exposed to a mildly hypoxic environment due to the typical 8,000-ft (565 mmHg) cabin pressurization of commercial aircraft (Pressurized Cabins, 2012; Muhm et al., 2007). The total amount of oxygen (O_2) available at this pressure is the equivalent of approximately 15% O_2 at sea level. Exposure to increasing elevations, and thus decreased available O_2, is known to induce Acute Mountain Sickness (AMS), an acute hypoxic condition typified by headache, weakness, nausea, and dizziness (Peacock, 1998; Roach et al., 2018), occurring with increasing frequency at higher altitudes. AMS is most often encountered by those who are not acclimatized to altitude; thus, infrequent flyers who live at lower altitudes are the most susceptible to experiencing AMS-like symptoms in flight. Altitude acclimatization, typified by an increase in hemoglobin and hematocrit, is an outcome of high-altitude exposure (Peacock, 1998; Wu et al., 2012) and has the physiological effect of enriching the amount of available O_2 in the blood.

Hypoxia stimulates a widespread transcriptional response centered on the hypoxia-responsive HIF1α protein. HIF1α, which is ubiquitinated and degraded at normoxia, is stabilized under hypoxia by hydroxylation of the O_2-sensing proteins PHD and FIH1, after which it acts as both an activating and repressing transcription factor in concert with an array of cooperating proteins (Semenza et al., 1997; Majmundar et al., 2010). In addition to serving as a primary transcription factor, HIF1α also activates additional transcription factors, including FOS, CREB, CEBPB, NFY, MIF, FOXO3, and E2 (Dengler et al., 2013; Seifeddine et al., 2008; Sermeus & Michiels, 2011; Licht et al., 2006). Hypoxia also upregulates *VEGF*, *ATM*, and other factors leading to increased cellular growth, immune recruitment, angiogenesis, and inflammation (Majmundar et al., 2010; Olcina et al., 2014). This results from the cellular drive to cope with a lack of O_2 by increasing glycolytic metabolism, mitigating the effects of reactive oxygen species (ROS) damage, increasing O_2 perfusion, and ultimately increasing oxygenation through an increase in blood supply (Sarkar et al., 2003; Baze et al., 2010; Kaur et al., 2010; Burki & Tetenta, 2013; Srinivasan et al., 2015).

Hypoxia, which induces a large-scale reallocation of cellular activities, is also known to induce changes in chromatin accessibility in several tissues (Melvin & Rocha, 2012). Mimura et al. (2012) found that HIF1α acts in concert with KDMA3 to demethylate lysine 9 of histone 3 at the target loci and serve to activate glycolytic pathways. Lee et al. (2017) discovered that both activating ($H3K4me^3$) and repressing ($H3K9me^3$ and $H3K27me^3$) trimethylations of histone H3 were altered in a gene-specific manner, and that transcription factor binding was enriched according to that change in chromatin state. Prickaerts et al. (2016) demonstrated an increase in both activating $H3K4me^3$ and repressing $H3K27me^3$ during severe hypoxia (< 1% O_2), as well as deactivation of histone demethylases.

Most published studies on chromatin alteration during hypoxia have relied on chromatin immunoprecipitation and chromatin immunoprecipitation sequencing (ChIP-seq) techniques,

which limit findings to the regions that bind the antibody or epitope used. The Assay for Transposase-Accessible Chromatin (ATAC-seq) is a method of examining global chromatin accessibility, using the euchromatic binding preference of the tagging Tn5 transposase to preferentially 'tag' nucleosome-free chromosomal regions and thereby assay the nucleosomal accessibility of the entire genome (Buenrostro et al. 2015). Thus, ATAC-seq may be used to globally examine changes in chromosomal accessibility according to condition, revealing nucleosome density along the entire genome. To determine the extent of change in chromatin accessibility during mild (15% O_2) and severe (2% O_2) hypoxia, we treated cultured human bronchial epithelial cells (HBECs) with a range of O_2 concentrations for 16 hours and performed ATAC-seq and microarray-based gene expression analysis. The findings of this study will provide information to develop future work in biomarkers, aerospace medicine, and pulmonary research. It will also be of use in exploring hypoxia-related DNA accessibility and gene expression changes.

Methods

Cell culture and treatment

HBECs were obtained from Lonza (Normal Human Bronchial Epithelium with Retinoic Acid, item CC-2540, lot 0000646466). All cells were collected from a single individual, identified as a 38-year-old Caucasian male. The cells were grown in Lonza Bronchial Epithelial Growth Medium with Retinoic Acid (BEGM, Lonza, item CC-3171) supplemented with a Lonza Bronchial Epithelial Growth Medium BulletKit (Lonza, item CC-3170) at 37°C, 5% CO_2 in a humidified growth chamber. Cells were started with 0.3 mL of primary culture and grown under the described conditions in 20 mL of medium until reaching 80% to 90% confluence, a period of approximately five days. The media was then removed, and cells were released from the flask with a pre-warmed Accutase solution (Sigma) and washed with 1X phosphate buffered saline. Cells were passed at 1:10 (2 mL of culture into 18 mL medium) into a new collagen-coated flask (50 mL), which was placed back into the growth chamber. This passage was also carried to 80% to 90% confluence and then passed again into a new flask at 1:10 using the previously-mentioned procedure (for 4 to 5 days). The final flask was carried to 80% to 90% confluence (4 to 5 days), after which the cells were trypan blue stained (100-µL 0.1% trypan blue into 400-µL cell suspension) and counted using a hemocytometer. One hundred thousand cells were aliquoted into each well of an O_2-sensing six-well plate (Oxodish OD6, PreSens, Germany) with 2 mL of BEGM and placed in the incubator to attach and resume normal activity for 24 hours. After 24 hours, an additional 1 mL of pre-warmed BEGM was added to each well, and the six-well plate was placed in a humidified incubation box (Coy Laboratory Products, MI, USA) within a hypoxia chamber (Coy Laboratory Products, MI, USA) for 16 hours at either 20.8% (21pct), 15% (15pct), or 2% (2pct) O_2. O_2 concentration in solution was assessed with a SensorDish reader (SDR-382, PreSens) set for one reading every 15 minutes for the duration of the treatment. Upon completion of the treatment, plates were removed from the humidity box but

kept in the hypoxia chamber to maintain the cells at the treatment O_2 state while performing cleanup and nuclear extraction manipulations.

ATAC-sequencing

Forty thousand cells were removed from three of the six wells of the treatment plate after counting by hemocytometer and placed into individual 1.5-mL tubes for each replicate. Nuclei were extracted from each replicate according to Corces et al. (2017), an improved protocol designed to reduce the percentage of mitochondrial reads. Nuclei were then treated with Tn5 transposase (Illumina Nextera DNA Library Kit) to selectively cut and label open chromatin regions with sequencing adapters. The tagged fragments were amplified with dual-indexed primers (i7 and i5 primers, Illumina Nextera Index Kit) using an optimized thermal amplification profile (72°C 5 m, 98°C 30s, (98°C 10s, 63°C 30s, 72°C 60s) x 11 cycles, 72°C 5m, 4°C forever) and then purified using a 1:1 ratio of Ampure XP beads. Index primer combinations were selected using Illumina sample pooling guidelines. The washed and purified sample was eluted in 23 µL of elution buffer (Qiagen) and pooled for sequencing on one high-output Nextseq 500 flowcell (Oklahoma Medical Research Foundation Clinical Genomics Core Facility), producing 2x75 paired-end reads (2x75). ATAC-seq raw data were deposited into the NCBI Sequence Read Archive under bioproject accession number PRJNA 492498.

Microarray analysis

Affymetrix Human Transcriptome Array 2.0 (HTA 2.0) microarrays were used to analyze gene expression of the cellular population from the three wells of each six-well treatment plate not used for ATAC-seq. The entire cellular population for each well used in microarray analysis was suspended in 250 µL of Qiazol reagent (Qiagen) and placed at -80°C. Ribonucleic acid (RNA) was extracted from cellular samples using RNeasy mini kits (Qiagen) on the QIAcube® automation platform. RNA quality was assessed using RNA 6000 Nano kits (Agilent) on a Bioanalyzer 2100 (Agilent). RNA sample concentrations were determined using a NanoDrop 2000. Then, RNA samples were amplified using the Affymetrix GeneChip® WT PLUS Reagent Kit (Thermo Fisher Scientific). The concentration of single-stranded complementary DNA (cDNA) produced by amplification was measured using a NanoDrop 2000. Single-stranded cDNA was fragmented, labeled, and hybridized (Thermo Fisher Scientific GeneChip® WT PLUS Reagent Kit and GeneChip® Hybridization, Wash, and Stain Kit) onto Affymetrix GeneChip Human Transcriptome Assay 2.0 microarrays (Thermo Fisher Scientific) for analysis. Microarrays were hybridized for 18 hours, rotating at 60 rpm at 45°C. Chips were then washed and stained using two GeneChip® fluidics station 450 (Affymetrix) using protocol FS450-0001, per the HTA 2.0 microarray protocol. Stained and washed microarrays were scanned using a 7G GeneChip® Scanner 3000 (Affymetrix). Microarray raw and normalized data were deposited in the NCBI Gene Expression Omnibus database under accession number GSE121773.

ATAC-seq differential peak analysis

Raw fastq files were processed through the official Encyclopedia of DNA Elements ATAC-seq pipeline (Kundaje, 2020) using the following modifications from default parameters: adapter detection TRUE (using Illumina adapter sequence CTGTCTCTTATA), IDR=TRUE, peak selection p= 0.01, pooled peak pval= 0.05. The pipeline output files used for downstream analysis were pooled narrowpeak bed files, pooled count-normalized BigWig files, and individual bam files. The union of the pooled narrowpeak files was obtained with the Bedops software package (Neph et al., 2012), and the resulting union bed file was converted to .saf format using a custom script for use as an annotation file during the read counting step. Feature counting was performed using the Subread package (Liao et al., 2013; Liao et al., 2014), including bam files derived from each biological replicate. The resulting feature counts table was counts per million-normalized (CPM) using the R/edgeR software package and filtered to eliminate rows with normalized read sums of less than two across the row. The differential expression threshold was set at a false discovery rate of < 0.05 (Benjamini-Hochberg). Top differentially expressed genes for each contrast were determined according to the following criteria: log2 fold change (LFC) >|0.5| and false discovery rate (FDR) < 0.05 (Benjamini-Hochberg adjusted p-value, R/edgeR 3.7 software, Robinson et al., 2010; McCarthy et al., 2012). Differential expression was assessed across the following contrasts: 15pct - 21pct (15v21), 15pct - 2pct (15v2), 2pct - 21pct (2v21). These contrasts allowed the intuitive observation of upregulation and downregulation according to the severity of the hypoxic state. BEDTools (Quinlan, 2014) intersect was used to extract peak intersections for ATAC-seq:Microarray comparison, BEDTools subtract was used to extract unique peak lists for each treatment. Peak annotation was performed using Hypergeometric Optimization of Motif EnRichment (HOMER, Heinz et al., 2010) annotatePeaks.pl script with the current hg38v21 annotation file. Read densities were visually examined using BigWig and bam files in Integrated Genome Viewer (IGV, Robinson et al., 2011; Thorvaldsdottir et al., 2013)

The Fraction of Reads in Peaks (FRiP) was calculated by comparing the total number of filtered reads mapping to each peak in the merged peak file by DeepTools (Ramírez et al., 2016). DeepTools was used to generate heatmaps (computeMatrix and plotHeatmap) on gene sets representing unique peaks, differentially expressed peaks, observed transcription start sites, and all annotated genes in the hg38.v21 human genome annotation .gtf file.

Motif analysis

Unique peaks in each treatment were processed through the HOMER software package (Heinz et al., 2010) to discover motif enrichment (using the perl script findMotifsGenome.pl, with the 21pct treatment as background to compare 15pct and 2pct (15v21, 2v21), and 2pct treatment as background to compare 15pct treatment (15v2). HOMER v4.10 (Heinz et al., 2010) was also used to annotate peaks derived from the initial peak-calling pipeline (annotatePeaks.pl). The motif search was limited to 200 bases upstream and downstream from the peak center to analyze the proximity of peaks to genome features.

Microarray bioinformatics analysis

Microarray bioinformatics analysis was conducted using the Affymetrix Transcriptome Analysis Console (TAC, Affymetrix), a proprietary software package that uses the R package limma (Ritchie et al., 2015) to conduct differential expression analysis of microarray data. Raw .cel files were imported into the software analysis space and the following contrasts set: 15pct - 21pct (15v21), 15pct - 2pct (15v2), and 2pct - 21pct (2v21). Analysis settings were as follows: Probe Detection threshold requirement was 50% of samples expressing at least 5% above background, Area Under Curve (AUC) threshold 0.7, genome hg19, annotation HTA-2_0.r3.na36.hg19.a1.transcript.csv, and Map file HTA-2_0_MappingFile.r1.map. Also, RMA-SST normalization and transformation were used to normalize .cel files, gene-level FDR threshold was set to 0.05, and Ebayes analysis of variance was the statistical comparison method. Microarray quality assessment and differential expression analysis were performed within TAC. The quality assessment consisted of examining labeling and hybridization control probe intensities, positive vs. negative AUC, and signal box plots were used for raw and normalized signal intensities. All plots were generated in TAC.

Determining microarray-ATAC peak concordance

To relate chromatin accessibility to gene expression, we isolated the significantly differentially expressed (DE) promoter-transcription start site (TSS) localized peaks from each comparison and compared their chromosomal locations to the chromosomal coordinates of each significantly DE gene annotation from corresponding microarray analysis. First, as the microarray-derived chromosomal coordinates were based on the hg19 genome, the coordinates were converted from hg19 to hg38 using the web-based NCBI Genome Remapping Service (https://www.ncbi.nlm.nih.gov/genome/tools/remap). Then, to capture peaks binding upstream of the transcription start site, we extended each microarray-derived chromosomal location by 3,000 bases upstream. Each coordinate file was compared using BEDTools intersect, which determined areas of intersection between each file. The resulting intersections were then annotated using the HOMER annotatePeaks.pl script.

Results and Discussion

ATAC-seq

To assay variation in chromatin accessibility in identical populations of bronchial epithelial cells according to O_2 availability, bronchial epithelial cells from a single individual under three different O_2 regimes: 21.8% (21pct), 15% (15pct), and 2% (2pct), as measured in solution. The treated cells were harvested and subject to Omni-ATAC-sequencing, a modified ATAC-seq protocol designed to reduce mitochondrial DNA contamination of the sequencing read pool (Buenrostro et al., 2015; Corces et al., 2017). ATAC libraries were sequenced to a depth of approximately 70 to 90 million paired-end reads per replicate after quality filtering, including filtering by read quality, mapping quality, duplication, and mitochondrial mapping (Table 1).

Table 1

ATAC-sequencing and Quality Metrics

Treatment_Rep	2pct_1	2pct_2	2pct_3	15pct_1	15pct_2	15_pct_3	21pct_1	21pct_2	21pct_3
Total Reads	69,136,462	73,555,984	68,148,932	90,661,196	92,953,290	88,259,166	77,670,220	76,363,386	77,602,234
Pct Mapped (Not Filtered)	99.60	99.63	99.70	99.67	99.61	99.66	99.65	99.63	99.66
Filtered Reads	49,992,082	49,788,704	48,762,496	56,900,854	46,039,854	42,901,538	60,965,232	61,250,378	62,293,586
Pct Mapped (Filtered)	100	100	100	100	100	100	100	100	100
Mitochondrial Read Percentage	10.1	15.3	11.7	21.4	36.3	37.7	2.2	0.8	1.3
Non-Redund. Fraction	0.98	0.97	0.97	0.97	0.97	0.97	0.96	0.97	0.97
PCR Bottleneck Coefficient 1	0.97	0.97	0.97	0.97	0.97	0.97	0.96	0.97	0.97
PCR Bottleneck Coefficient 2	41.82	39.49	38.44	36.32	31.95	33.78	23.90	32.70	34.48
TSS Enrichment	7.12	7.50	4.74	7.63	11.34	11.02	8.11	4.86	3.93
NFR/MonoNuclear Reads	3.23	3.77	3.91	3.42	4.37	4.34	2.54	4.49	4.17
Fraction of Reads in NFR[2]	0.64	0.67	0.67	0.64	0.68	0.69	0.57	0.69	0.66
Median Fragment Size[1]	500	500	500	462	462	462	471	471	471
Reads Mapped to Peaks	5,594,886	5,966,360	4,362,382	8,829,612	10,628,924	9,641,166	8,850,074	5,670,842	5,469,034
% Mapped to Peaks (FRiP)*	11.19	11.98	8.95	15.52	23.09	22.47	14.52	9.26	8.78

1. Median Fragment size calculated per treatment. 2. Nucleosome-Free Regions. This statistic details the fraction of reads mapping to nucleosome-free regions, which are constitutively open-chromatin regions. *Percentage of reads mapped to union peak file.

Note. ATAC = Assay for Transposase-Accessible Chromatin; FRiP = Fraction of Reads in Peaks; NFR = Nucleosome-free region; pct = percent; PCR = polymerase chain reaction; TSS = transcription start site.

Fastq quality control reduced the number of reads by approximately 20%, and 100% of the filtered reads in each replicate mapped to the human genome (hg38 v21). Between 8.78% and 23.09% of the filtered sequencing reads in each replicate mapped to the union peak list. The percentage of reads mapping to the union peak list was uniformly greater in the 15pct treatment than in the 2pct or 21pct treatments, as was the percentage of mitochondrial reads (Table 1). Mitochondrial reads exhibited low proportions in all samples but were lowest in the 21pct O_2 samples (2.2% to 0.8% of total reads, Table 1). This low percentage of mitochondrial reads was independently confirmed by running a second set of 21pct replicates from an additional individual (data not shown), not included in further analyses due to its divergent genotype. Tiede et al. (2011) found that cytoplasmic mitochondrial fractions rise, but mitochondrial activity decreases as O_2 levels decrease. Thus, the increase in mitochondrial reads observed in the present study may result from an increase in the mitochondrial fraction under the 15pct and 2pct O_2 treatments.

Peak Calling and Differential Peak Expression Analysis Reveal Chromatin Accessibility Differences Between Oxygen Treatments

Peak calling was performed with Model-based Analysis of ChIP-Seq (MACS2) software, narrow peaks were assessed by comparing all replicates for each treatment and determining the treatment-specific consensus peak set. Peaks (chromosomal regions with read density significantly above background) were identified using a p-value cutoff of < 0.01. Each treatment produced different numbers of called peaks; the 21pct treatment yielded 135,098 peaks, the 2pct treatment yielded 124,718 peaks, and the 15pct treatment produced 176,085 peaks. Annotation of these peak files using the annotaterPeaks.pl script from the HOMER software package showed that the annotation profiles were largely equivalent for all treatments, with the greatest percentage of peaks in each treatment being located in intergenic or intronic regions (Figure 1). The percentage of peaks lying within promoter regions was greatest in the 2pct treatment (15%), followed by the 21pct treatment (14%), and finally by the 15pct treatment (12%). The 2pct treatment also displayed a larger percentage of peaks lying within 5' untranslated region (5' UTR) regions (2%) than either of the other treatments (1% each). The 2pct treatment had fewer peaks lying within non-coding RNA (ncRNA) regions (< 0.5%) than either the 21pct or 15pct treatments. The remaining classifications had identical or very similar peak allocations.

Peaks unique to each treatment and in common to all were determined using BEDTools subtract. The 21pct treatment produced 19,029 unique peaks, the 15pct treatment produced 47,782 unique peaks, the 2pct treatment produced 20,172 unique peaks, and all treatments shared 97,924 peaks in common. Examination of the consensus peak intensity (BigWig) signals produced from each treatment (Figure 2) reveals that these unique peaks exist in each treatment, but at a sub-significant level. Globally, individual ATAC peak intensity varied little between treatment (Figure 2A). Viewed individually, however, differences in peak height were

visible. A selection of significant promoter-localized DE peaks for each treatment revealed apparent differences in peak intensity between the treatments (Figure 2B).

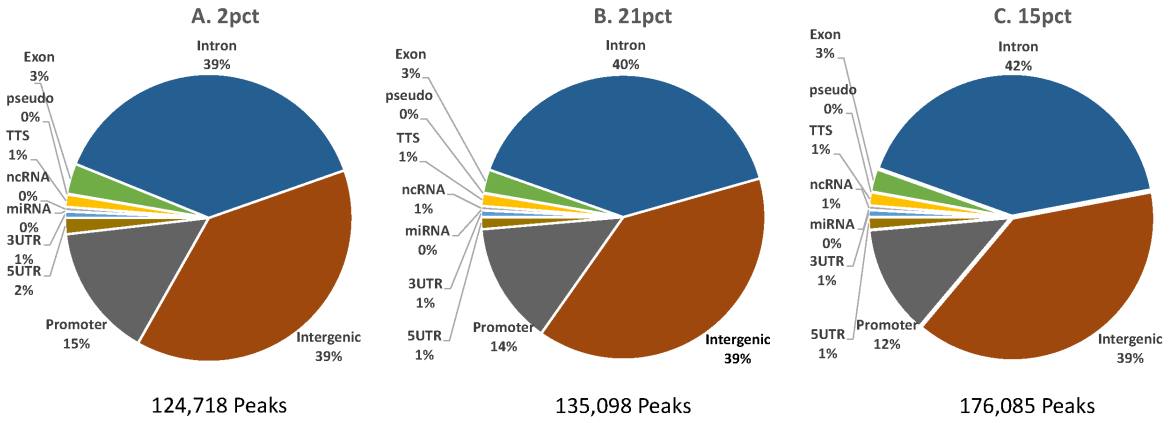


Figure 1. Distribution of peaks among gene features in consensus peak lists for each treatment.

The genomic location of each peak in the consensus peak lists for the 2pct, 15pct, and 21pct conditions were determined by the HOMER software package using the annotatePeaks.pl script. The majority of peaks in all conditions are located in intergenic and intron regions in each case. The proportion of peaks located in promoter and 5' UTR regions was greater in the 2pct treatment than the 15pct or 21pct treatments. A. Distribution of 124,718 called peaks in cells treated at 2pct O_2. B. Distribution of 135,098 called peaks in cells treated at 21pct O_2. C. Distribution of 176,085 called peaks in cells treated at 2pct O_2. TTS = Transcription Stop site, pseudo = pseudogene, ncRNA = non-coding RNA, 5UTR = 5’ untranslated region, 3UTR = 3’ untranslated region, miRNA = microRNA, Promoter = promoter localization combined with TSS localization.

Consensus peak sets for each treatment were then used as input to produce a union peak set by determining the union of each peak set, resulting in a file with 184,907 individual peaks (Supplementary Table 1). It should be noted that the absence of a called peak in a given consensus file does not denote the absence of within the peak region, as reads map to each of the noted regions in all samples, although their incidence does not rise significantly above background (Figures 2B and C). Filtered reads from each replicate were mapped against the union .bed file to determine the expression of each peak and also the extent of differential expression between treatments. The union peak file was converted to a .saf annotation file by a custom script, which was used for feature counting by the Subread software package. The resulting feature counts table of raw read counts per peak location was used as the basis to determine differential expression between each treatment (R/edgeR).

To determine significant differences in chromatin accessibility between treatments, we CPM-normalized and contrasted the treatments using the Subread-generated feature counts table with the R/edgeR package (Supplementary Table 2). As the significance of each peak against the background of each treatment was established in the initial peak calling process, only six peaks

were eliminated by introducing an additional filtering requirement of a row sum of at least two for each peak among the CPM-normalized reads. The specific contrasts were 15v21 (15pct minus 21pct), 15v2 (15pct minus 2pct), and 2v21 (2pct minus 21pct). Thus, we used the normoxic 21pct as the basis for comparison with the two hypoxic treatments, and then examined the true change in expression in the 15pct treatment in comparison to the 2pct treatment (15v2).

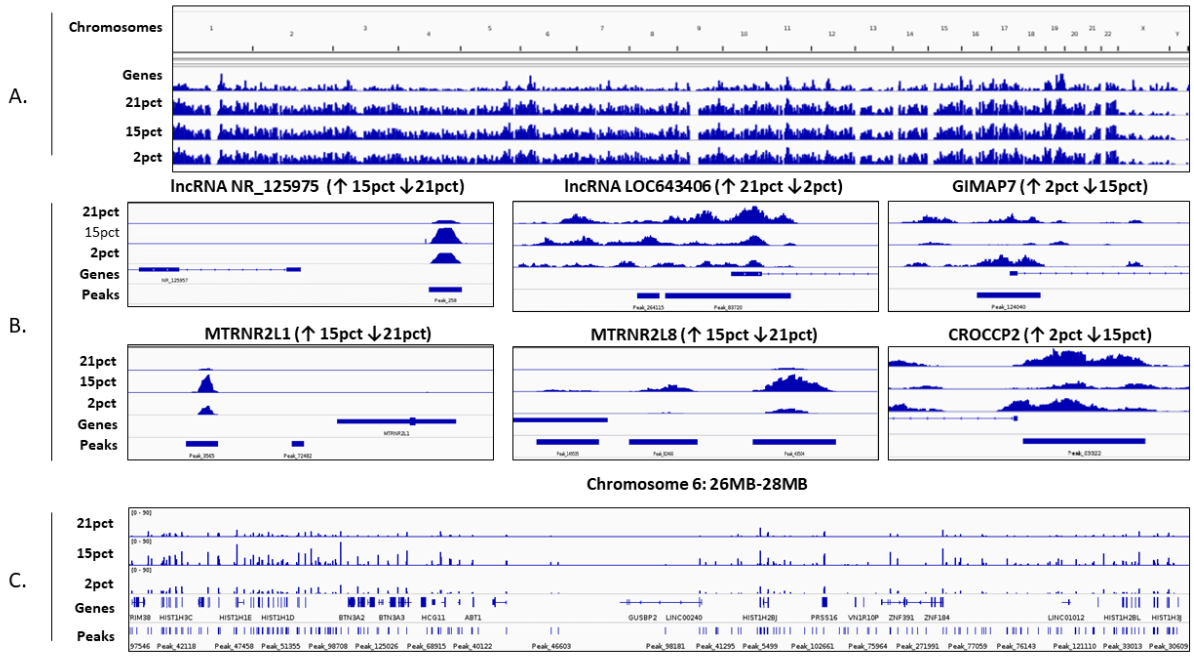


Figure 2. Visualization of peak distribution and read density according to genomic coordinate. A. Distribution of called peaks within the entire human genome (hg38). Chromosomes (1-22, X, and Y) are represented atop the chart. B. Visualization of read density (bigwig files) for each treatment at DE peaks. DE in 15vs21 comparison: lncRNA NR_125975, MTRNR2L1, MTRNR2L8. DE in 15v2 comparison: CROCCP2, GIMAP7. DE in 2v21 comparison: lncRNA LOC643406. C. Distribution of reads within bases 26,000,000 to 28,000,000 of chromosome 6, a region containing histone genes upregulated under 15% O_2 treatment. Peaks = peaks within combined peak file for all treatments (union peak file). Genes = binned density of annotated genes within each indicated chromosome. 21pct, 15pct, and 2pct (In Figure 2A)= binned density of called peaks within each treatment at all chromosomes. 21pct, 15pct, and 2pct (In Figure 2B and C)= density of reads within each treatment at indicated locations (scales within each image are identical).

The similarity of log-CPM normalized counts among treatments and replicates was examined using multi-dimensional scaling (MDS, similar to principal components analysis) using the R/edgeR software package (Figure 3D). Each of the three replicates for all treatments localized together, although the 15pct and 21pct treatments each displayed one replicate that lay apart from the other two, but still closer to their treatment group than to any other treatment group.

This was also reflected in the variability between replicates in Table 1. As the replicates grouped together, the decision was made to retain all replicates and proceed with further analysis.

R/edgeR analysis of differential chromatin accessibility (Table 2, Figure 3A-C, Figure 4A) between O_2 conditions revealed that the 15pct treatment elicited the greatest change in chromatin accessibility from the 21pct state, with a bias toward decreased chromatin accessibility (7,822 upregulated peaks, 17,998 downregulated peaks; Supplementary Table 3). The 15pct treatment displayed a similar relationship with the 2pct treatment, with 10,587 upregulated and 22,354 downregulated peaks (Supplementary Table 4). However, contrasting the 2pct and 21pct treatments revealed the upregulation of only 43 peaks and downregulation of 26 peaks (Supplementary Table 5).

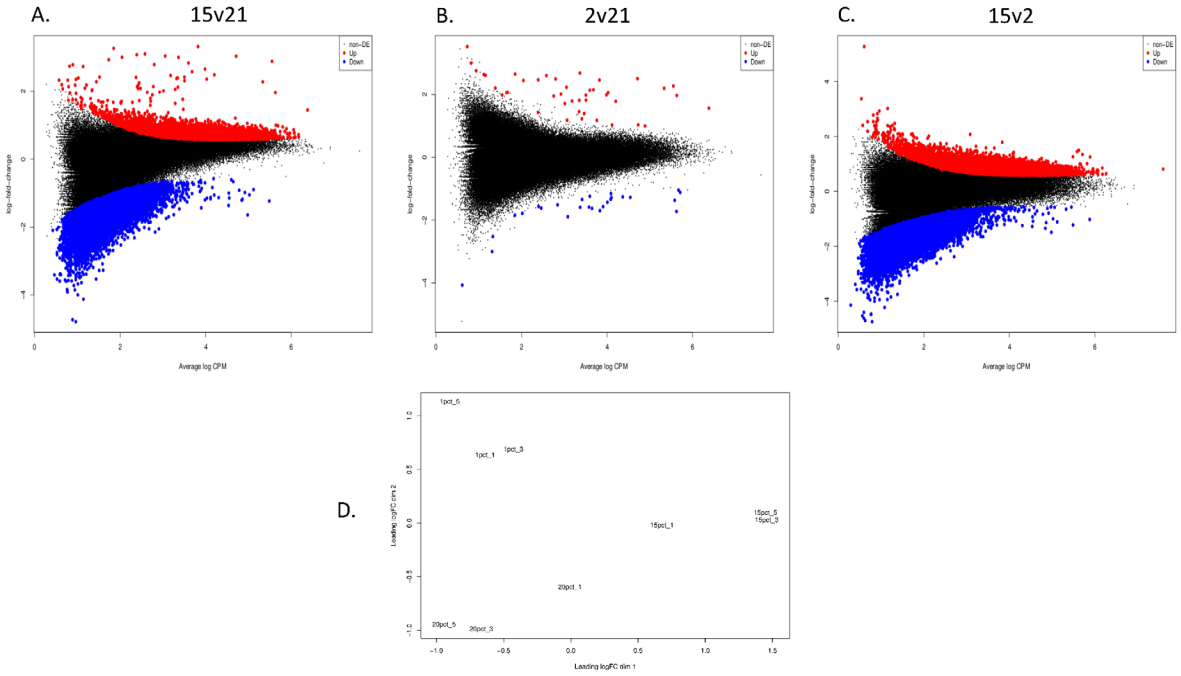


Figure 3. MA plots examining contrasts between each treatment and principal component analysis of all log-CPM normalized datasets for each treatment. A-C. MA plots of average expression (log CPM) of each peak in union peak list vs. log fold change of each peak according to the indicated contrast. A. 15pct treatment vs 21pct treatment. B. 2pct treatment vs 21pct treatment. C. 15pct treatment vs. 2pct treatment. D. PCA plot of log-CPM transformed feature counts for each called peak.

In examining peak chromosomal localization within genomic features, we determined that the majority of DE peaks among all contrasts lay within introns or in intergenic regions (Table 2). These DE peaks were largely downregulated in the 15pct treatment in comparison with both the 2pct and 21pct treatments. Intergenic and intronic DE peaks were generally upregulated in the 2pct treatment when compared to the 21pct treatment. The next-largest percentage of DE peaks in each contrast were localized to promoter/TSS regions. The majority of DE

promoter/TSS-localized peaks were upregulated in the 15pct treatment in contrast with the 21pct (791 up, 278 down) and 2pct (615 up, 579 down) treatments, and also upregulated in the 2pct vs 21pct contrast (10 up, 0 down). The 10 upregulated promoters in the 2pct vs 21pct contrast belonged to the genes *MTRNR2L1*, *ENO-AS1*, *AGRN*, *KIF13A*, *ADAMTS20*, *RCOR2*, *CMIP*, *ZNF84*, *LOC101928626*, and the unannotated NR_039666 (previously annotated as MIR4461, but removed and permanently suppressed by NCBI due to its removal from the micro RNA (miRNA) database miRbase due to RNAseq evidence that it is not an miRNA). Of the significantly more-accessible promoters in the 2pct treatment, only two have known roles in hypoxia; the anti-apoptotic *MTRNR2L1* (Yen et al., 2013) and the HIF1α-binding *RCOR2* (Ortiz-Barahona et al., 2010).

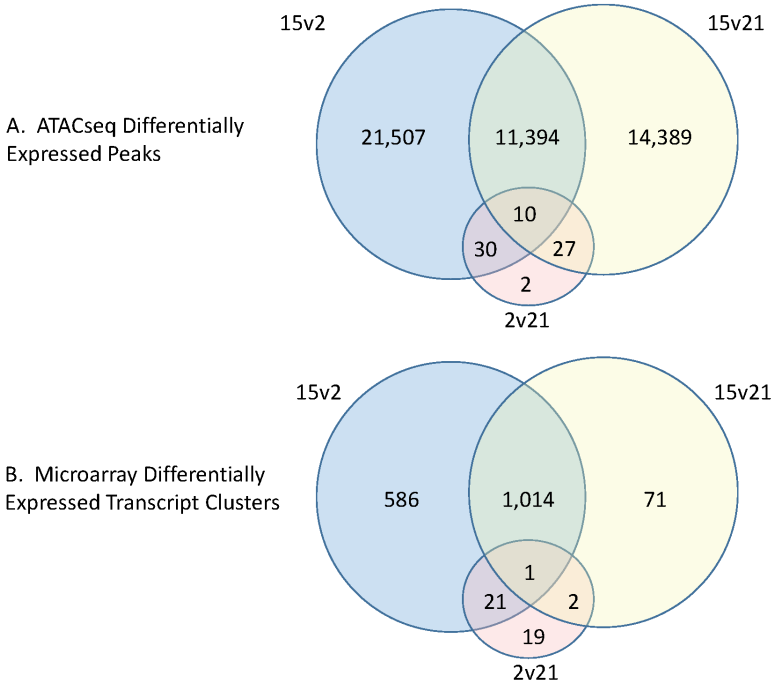


Figure 4. Venn diagrams of ATAC-seq and microarray differential expression results. A. ATAC-seq DE peak Venn diagram. B. Microarray DE gene Venn diagram. Contrasts are indicated for each peak or gene pool.

The global decrease in chromatin accessibility among DE peaks in the 15pct treatment in all comparisons suggests a large-scale chromatin rearrangement at 15% O_2. In contrast, the lack of significant difference between the 21pct and 2pct treatments suggests that the strong activation of a select subset of genomic locations may act to avoid the necessity for such large-scale rearrangement. Further, the absence of known hypoxia-mediating locations from the 10 upregulated promoter regions in the 2pct vs. 21pct contrast suggests that hypoxia-regulated locations may be constitutively accessible in bronchial epithelium. The accessibility decrease observed in the 15pct treatment also demonstrates that differential expression is not dependent on peak calling. If unique peaks in each treatment were always significantly upregulated only in the treatment of origin, most of the upregulated peak set in each treatment

would consist of its unique peaks, and most downregulated peaks in each peak set would consist of peaks unique to the other two treatments. This was not observed, suggesting that the changes seen herein are valid.

ATAC-seq Signals Display Differences According to Expression

To examine chromatin accessibility within transcription start sites, we isolated a TSS list with at least one called peak within 1,000 bases up- or down-stream of that TSS (n= 13,925). Examination of consensus BigWig signals from each treatment (Figure 5) revealed a globally stronger signal in the 15pct treatment (Figure 5A). This data coincided with the observation that transcription start sites were preferentially upregulated in the 15pct treatment (Table 2).

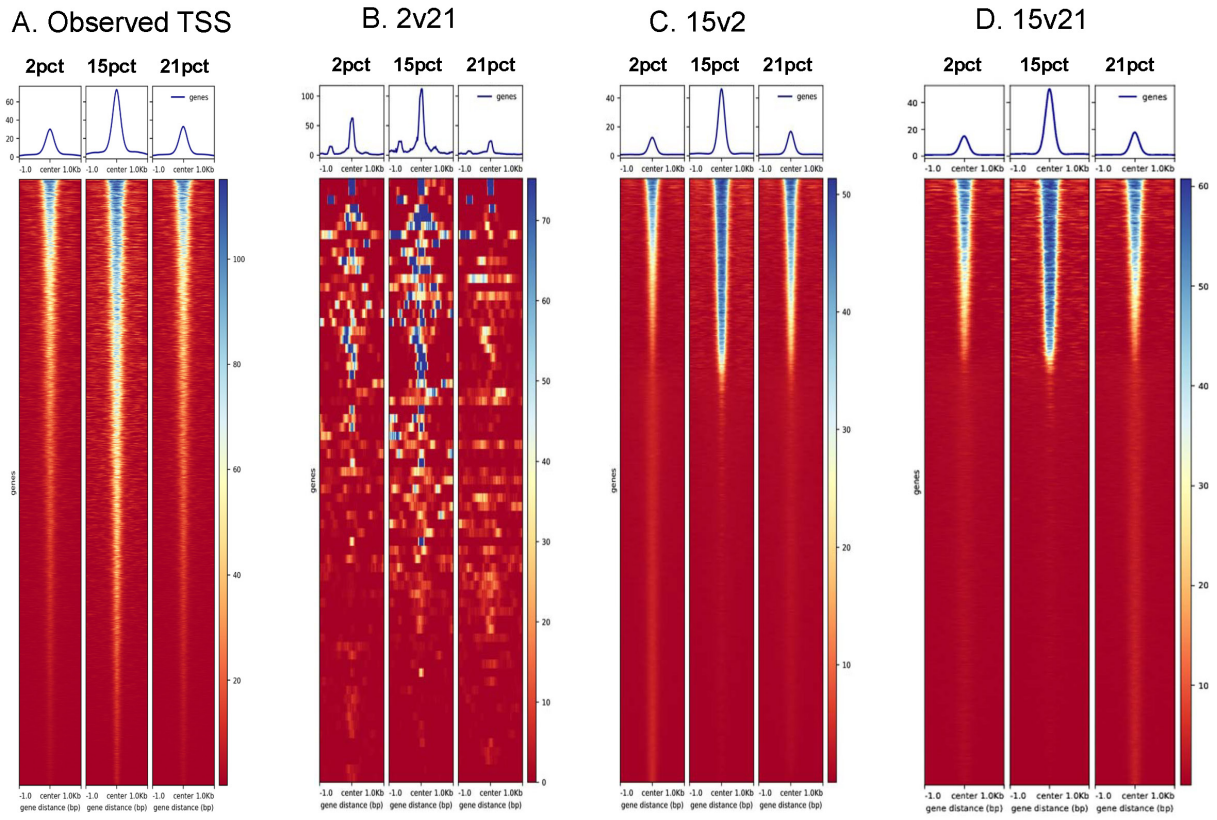


Figure 5. Heatmaps examining consensus read distribution within 1,000 bases of transcription start sites and within 1,000 bases of each differentially expressed peak for each indicated contrast. Intensity scales are located to the right of each heat map. A. Peak distribution within 1,000 bases of all observed transcription start sites. B. Distribution of read density around DE peaks in 2pct vs. 21pct contrast. C. Distribution of read density around DE peaks in 15pct vs. 2pct contrast. D. Distribution of read density around DE peaks in 15pct vs. 21pct contrast.

To examine the distribution of peaks in relation to gene features, we extracted all gene coordinates (n= 50,381 individual genes) from the hg38.p12 annotation file (gencode.v28.annotation.gtf) and mapped consensus BigWig peaks along each gene (Figure 6) with and without k-means clustering (clusters set to 3 to capture potential unique peak

Table 2

Differentially Expressed Peaks in ATAC-seq Comparisons According to Genomic Location

Annotation	15v21				15v2				2v21			
	Peaks	% of Peaks	Up	Down	Peaks	% of Peaks	Up	Down	Peaks	% of Peaks	Up	Down
Non-coding	193	0.8	64	129	234	0.7	79	155	0	0.0	0	0
Intergenic	12,534	48.5	3,155	9,379	15,727	47.7	4,346	11,381	32	46.4	17	15
Intron	10,891	42.2	3,478	7,413	14,228	43.2	5,160	9,068	20	29.0	14	6
TTS	292	1.1	138	154	388	1.2	172	216	5	7.3	1	4
Exon	590	2.3	81	509	838	2.5	82	756	1	1.4	1	0
Promoter-TSS	1,069	4.1	791	278	1,194	3.6	615	579	10	14.5	10	0
3'	171	0.7	61	110	218	0.7	89	129	0	0.0	0	0
5'	80	0.3	54	26	114	0.4	44	70	1	1.4	1	0
Total	25,820	100	7,822	17,998	32,941	100	10,587	22,354	69	100	44	25

Note. ATAC = Assay for Transposase-Accessible Chromatin; TSS = transcription start site.

instances between treatments). Mapping signal intensities along gene locations did not reveal any noticeable difference in gene accessibility between treatments. K-means clustering also displayed no apparent differences between treatments within clusters. Signals were split broadly into three separate groups; the first displaying strong ATAC peaks only at the transcription start site, the second displayed whole-gene accessibility progressing to peaks centered around the transcription start site, and a third with weak ATAC signals scattered widely upstream and downstream of the transcription start site, progressing to a weak ATAC signal centered around the TSS. The lack of clear separation between treatments according to transcription start site peak localization showed that, on a large scale, the treatments have very similar chromatin profiles.

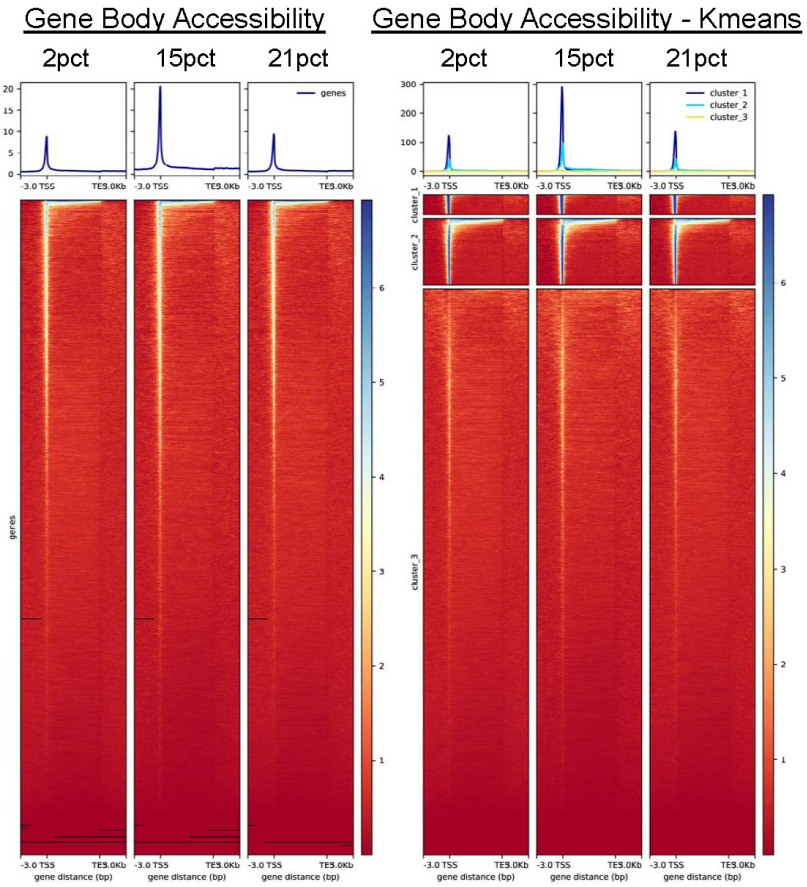


Figure 6. Heatmaps examining gene body read density. All annotated genes from hg38v21 annotation are represented. Intensity scales indicated at the right of each heatmap.

Gene Expression Analysis by Microarray

Microarray analysis was performed on cells from three wells of the original six-well treatment plates. One 21pct replicate failed the initial quality assessment and was excluded from further analysis. The remaining samples were hybridized on Affymetrix HTA 2.0 Human Transcriptome

microarrays, and the resulting data were analyzed using the Affymetrix Transcriptome Analysis Console using contrasts identical to those performed for differential ATAC peak detection. The 15pct treatment yielded consistently higher expression among the majority of differentially expressed genes in contrast with the 21pct and 2pct treatments (Figure 7, Supplementary Tables 6 and 7). Eighty-seven percent (944 genes) of the 1,088 DE genes between the 15pct and 21pct treatments were upregulated in the 15pct treatment (Figure 7A, Supplementary Table 6). Among the 1,622 DE genes between the 15pct and 2pct O_2 treatments, 80% (1,285 genes) were upregulated in the 15pct treatment (Figure 7C, Supplementary Table 7). Notably, many fewer DE genes (n=43) were noted when contrasting the 2pct and 21pct treatments, with 19 genes upregulated and 24 genes downregulated in the 2pct treatment when compared with the 21pct treatment (Figure 7B, Supplementary Table 8). Interestingly, the 15pct treatment demonstrated the significant upregulation of 38 histone genes in the 15v2 contrast and 22 histone genes in the 15v21 contrast. This finding provides supporting evidence for the observation of a large decrease in chromatin accessibility in the 15pct treatment, and an explanation for the increase in called peaks and fraction of reads in those peaks in the 15pct treatment when each treatment contained very similar numbers of filtered reads.

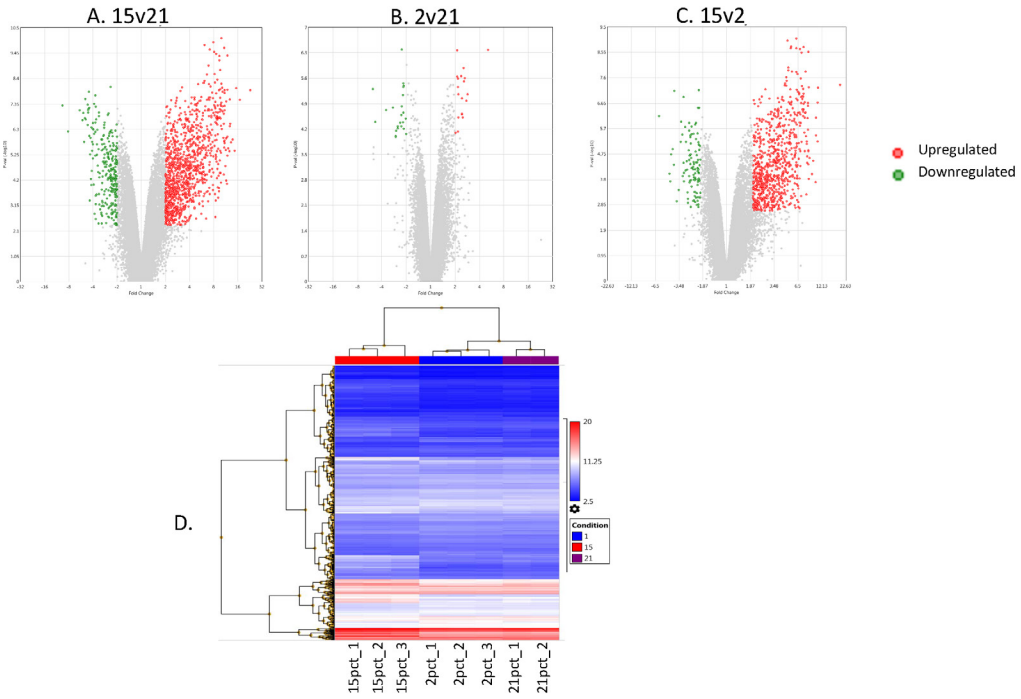


Figure 7. Microarray gene expression measurement contrasted according to treatment. A. Volcano plot examining -log10 p-Value vs. fold change of expression in 15pct vs. 21pct contrast. B. Volcano plot examining -log10 p-Value vs. fold change of expression in 2pct vs. 21pct contrast. C. Volcano plot examining -log10 p-Value vs. fold change of expression in 15pct vs. 2pct contrast. D. Unsupervised hierarchical clustering by expression value for differentially expressed genes across all treatments. Key and intensity scale located at the right of the chart.

Comparisons of the DE genes generated by each contrast (Figure 4A and 4B) revealed that only one gene, angiopoietin-like 4 (*ANGPTL4*), an angiogenic lipoprotein lipase inhibitor regulating fatty acid transport to cells (Gusarova et al., 2018), was declared significant in all comparisons; downregulated in both 15pct contrasts, but upregulated in the 2v21 contrast. The 15v2 contrast found 586 DE genes not observed in any other comparison, 1,014 in common with the 15v21 contrast, and 21 in common with the 2v21 contrast. The 15v21 contrast contained 71 significant DE genes not shared with any other contrast and shared two significant genes with the 2v21 contrast. The 2v21 contrast contained 19 unique DE genes. The 1,014 shared DE genes between the 15v2, and 15v21 contrasts may be specifically regulated by mild hypoxia; the 586 and 71 unique genes in either 15pct contrast may be due to genes specifically responsive to severe hypoxia (in the 15v2 contrast) and mild hypoxia (in the 15v21 contrast). The 19 unique genes in the 2v21 contrast may be responsive specifically to severe hypoxia.

Concordance Between Differentially Expressed Genes and Peaks Reveals Upregulation of Histones in 15pct Treatment

To establish concordance between the DE ATAC-seq peaks and microarray-assessed DE genes, we determined the intersecting genomic coordinates of those DE peaks and genes in each dataset. Chromosomal coordinates of promoter/TSS localized peaks from each comparison were compared to the chromosomal coordinates of each significantly DE gene annotation from corresponding microarray analysis. Comparing the 2v21 DE peaks and DE genes resulted in one intersecting region, in the intergenic region 4,956 bases downstream of the DE gene *NFKBIA* (Supplementary Table 9). *NFKBIA* (NFκB Inhibitor Alpha) is directly involved in the hypoxia response, supporting the observation that hypoxia is downregulated (LFC, -1.02) in the 2pct treatment. As *NFKBIA* inhibits the pro-inflammatory and hypoxia-upregulated *NFκB* (Rao et al., 2011; Li, et al., 2017) during hypoxia, its downregulation may signal an increase in the ability of *HIF1α* to mediate the hypoxic response at 2% O_2.

Examining the concordance between the 15v21 ATAC-seq and Microarray DE datasets yielded 162 intersecting regions within 105 individual genes (Table 3, Supplementary Table 10). The majority of concordant peaks were associated with intergenic regions (31.3%), followed by promoter-TSS and intron regions (each 28.8%) and low numbers of TTS, exon, 5'UTR, 3' UTR, and non-coding designations. Of the 47 intersecting peaks localized to promoter regions, 11 fell in histone genes (*HIST1H2AD*, *HIST1H2AE*, *HIST1H2AG*, *HIST1H3B*, *HIST1H3I*, *HIST2H2AB*, and *HIST2H2AC*). All the concordant histone peaks were upregulated in the 15pct treatment in both the ATAC-seq comparison and the microarray comparisons. Additional promoter-localized concordant genes of interest included *SERPINE1*, a hypoxia-upregulated molecule responsible for tissue remodeling and implicated in fibrosis (Muth et al., 2011) that was downregulated in the 15pct treatment in comparison to both the 21pct and 2pct treatments. *PLXDC1* (referred to as uc021twq.1 in Supplementary Table 6), significantly upregulated in 15pct treatment, negatively regulates angiogenesis through binding *PEDF* (Cheng et al. 2014) and is thus

potentially involved in angiogenesis and in response to mild hypoxia, in agreement with the downregulation of *ANGPTL4*.

Table 3

Intersection between DE ATAC-seq Peaks and DE Genes

	15v21		15v2		2v21	
Annotation	**Total**	**Percentage**	**Total**	**Percentage**	**Total**	**Percentage**
intron	47	29.0	83	43.2	0	0
Intergenic	51	31.5	52	27.1	1	100
promoter-TSS	47	29.0	37	19.3	0	0
TTS	12	7.4	15	7.8	0	0
exon	2	1.2	2	1.0	0	0
5' UTR	1	0.6	1	0.5	0	0
3’ UTR	1	0.6	1	0.5	0	0
Non-coding	1	0.6	1	0.5	0	0
Gene Type						
ncRNA	37	22.8	40	20.8	0	0
Protein-Coding	103	63.6	124	64.6	1	100
Pseudogene	2	1.2	3	1.6	0	0
snoRNA	6	3.7	10	5.2	0	0
snRNA	13	8.0	14	7.3	0	0
Not Annotated	1	0.6	1	0.5	0	0

Note. ATAC = Assay for Transposase-Accessible Chromatin; DE = differentially expressed; ncRNA = non-coding ribonucleic acid; snoRNA = small nucleolar ribonucleic acid; snRNA = small nuclear ribonucleic acid; TSS = transcription start site; UTR = untranslated region.

Comparing the intersection of the 15v2 datasets found 192 concordant DE peaks aligning with 129 individual genes (Table 3, Supplementary Table 11). As in the other contrasts, the majority of concordant peaks were located within protein-coding genes, followed by ncRNAs, small nuclear RNAs, small nucleolar RNAs, and pseudogenes. Of the promoter-localized concordant peaks, nine were located within the promoter of the significantly upregulated histone genes *HIST1H2AL*, *HIST1H2BI*, *HIST1H3C*, *HIST1H4L*, *HIST1H3H*, *HIST1H3B*, and *HIST2H2AB*, all located on chromosome 6, except *HIST2H2AB* and *HIST2H2BF*, located on chromosome 1 (Figure 2C). The large-scale upregulation of histone genes in the 15pct treatment compared to both the normoxic and hypoxic conditions further confirmed the observed decrease in chromatin accessibility in the 15pct treatment. Visualization of the chromatin accessibility profiles of Chromosome 6:bases 26,000,000 to 28,000,000, where the majority of the concordant histone

genes are located, confirmed the increased accessibility of each histone gene contained within this region in the 15pct treatment (Figure 2C).

Thus, the microarray and ATAC-seq datasets support one another. The observed pattern of large-scale changes within the 15pct treatment in comparison to the 21pct and 2pct treatments was seen in both analyses. While the majority of DE peaks were downregulated in the 15pct treatment in contrast with both the 2pct and 21pct treatments, most downregulated peaks were observed in intergenic and intronic regions, whereas DE promoter accessibility increased, signaling increased transcription. Accordingly, microarray analysis also indicated large-scale upregulation of DE genes in the 15pct treatment, particularly among histone genes, potentially signaling an increase in chromatinization. While the increase in FRiP and TSS enrichment in the 15pct treatment was initially regarded with concern, our results suggest that these increases were the result of a widespread decrease in chromatin accessibility due to cellular growth at 15% O_2, with a resulting decrease in the percentage of the genome available for Tn5 transposition. The increase in FRiP in the 15% treatment may have resulted from a global decrease in chromatin accessibility, "focusing" the tagging transposase on a restricted number of nucleosome-free sites and thereby reducing background. The increase in mitochondrial reads in the 15pct and 2pct treatments may have resulted from an increase in the mitochondria in hypoxia, as noted by Tiede et al. (2011).

Pathway Analysis Predicts Downregulation of Proliferative Responses at 15pct O_2 and Upregulation of Hypoxic Response at 2pct O_2

To examine the significance of microarray-assessed differential gene expression between treatments, we submitted the lists of differentially expressed transcript clusters (Log Fold Change > |1|, FDR <0.05) to Ingenuity Pathway Analysis (IPA) for Core Pathway determination. Many of the DE transcript clusters localized to ncRNA, miRNA, pseudogenes, and other regulatory regions (Supplementary Tables 6, 7, and 8), thus possessed insufficient functional information for IPA to include them in the analysis. The 15v21 contrast produced 322 analysis-ready genes, the 15v2 contrast contained 475 analysis-ready genes, and the 2v21 contrast contained 32 analysis-ready genes.

Pathway analysis predicted several up-and downregulated upstream effectors confirming the general gene and peak expression patterns observed in the ATAC-seq analyses, with a general downward trend in the 15pct treatment (Table 4). Notably, downregulation of *HIF1α*, a definitive hypoxia-responsive factor (Semenza et al., 1997; Belaiba et al., 2007), was predicted in the 15pct treatment with both the 21pct and 2pct treatments, based on the direction of change of downstream molecules. *HIF1A* was not differentially expressed in any comparison; it approached significance (FDR= 0.0942; Supplementary Table 6) in the 15v21 comparison, although with a log fold change of only -0.26 (Figures 8A-C). The chromatin profile of *HIF1A* and its associated antisense regulators *HIF1αS1* and *HIF1αS2* revealed large peaks in all treatments at the promoters of *HIF1α* and *HIF1α-AS2*, although the peaks were not significantly different among any comparison (Figure 8D). The activation of *HIF1α* was expected in both the 15pct and

2pct treatments, and thus the downregulation of *HIF1α* in the 15pct in comparison with the 21pct treatment is surprising.

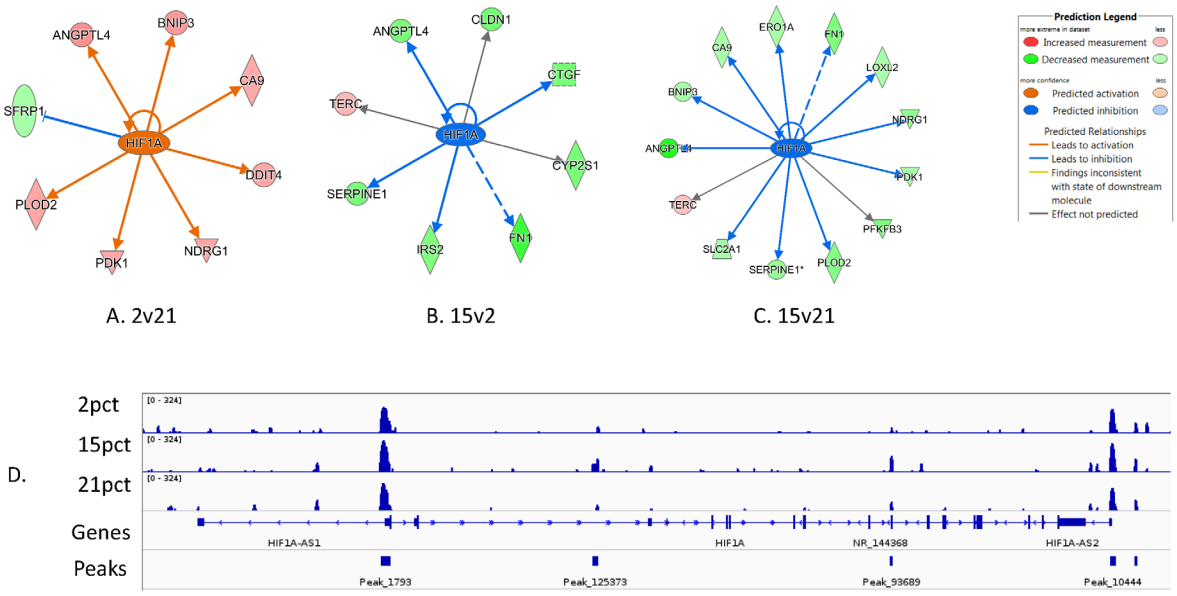


Figure 8. Examination of predicted *HIF1A* regulation and read density along *HIF1A* and associated antisense transcripts. A. IPA-predicted increase in *HIF1A* gene expression in 2pct treatment vs. 21pct treatment. B. IPA-predicted decrease in *HIF1A* expression in 15pct vs 2pct contrast. C. IPA-predicted decrease in HIF1A expression in 15pct vs 21pct contrast. D. Read density distribution within *HIF1A* and associated antisense (AS) transcripts. *HIF1A* was not among DE genes and had no associated DE peaks.

Comparison of the 15pct and 21pct treatments resulted in 20 significantly changed regulatory molecules, of which only three were activated, again confirming the trends observed in both the ATAC-seq peak analyses. *MAPK1*, *NEUROG1*, and *RARA* were activated in the 15pct treatment, while the remaining factors, including *HIF1A*, *NFKB*, and *ATM*, were all implicated in the hypoxia response, were inhibited (Table 4). Of the increased regulators, only *MAPK1* has displayed a clear role in hypoxia, increasing during intermittent and sustained hypoxia in rat's lungs (Wu et al., 2008). The role of *NGN1* in hypoxia is less clear; *NGN1* is downregulated by a decrease in *NOTCH1* signaling, which is, in turn, upregulated by hypoxia (Gustafsson et al., 2005). While *NOTCH1* was not among the significantly changed regulators in the 15v21 contrast, it was among the sub-significantly upregulated regulators in the 2v21 comparison (data not shown).

Table 4

Significantly Changed Upstream Regulatory Molecules

	Upstream Regulator	Molecule Type	Pred. Act. State	Activation z-score	p-value of overlap	Mechanistic Network
15v2	PRKAA1	kinase	Activated	2.20	6.65E-03	41 (6)
	DUSP1	phosphatase	Activated	2.00	5.03E-03	
	RICTOR	other	Inhibited	-3.74	1.33E-07	
	HIF1A	transcription regulator	Inhibited	-3.26	5.94E-06	45 (8)
	IL5	cytokine	Inhibited	-2.65	1.30E-03	
	NUPR1	transcription regulator	Inhibited	-2.55	7.76E-13	
	ARNT	transcription regulator	Inhibited	-2.41	1.23E-04	
	CD38	enzyme	Inhibited	-2.61	4.98E-04	
	SYVN1	Transporter	Inhibited	-2.24	8.00E-03	
	PGR	lig-dep nuc. rec.	Inhibited	-2.21	1.90E-02	
	ATF4	transcription regulator	Inhibited	-2.00	2.92E-02	
	TGFB1	growth factor	Inhibited	-3.46	1.91E-04	48 (8)
	TLR9	transmembrane receptor	Inhibited	-2.00	1.12E-01	
	ERBB2	kinase	Inhibited	-2.83	1.82E-03	24 (3)
	NEDD9	other	Inhibited	-2.83	1.21E-09	35 (6)
2v21	HIF1A	transcription regulator	Activated	2.77	3.14E-10	
	NEDD9	other	Activated	2.44	8.94E-13	
	STAT3	transcription regulator	Activated	2.21	3.15E-05	
15v21	NEUROG1	transcription regulator	Activated	2.00	2.99E-04	
	MAPK1	kinase	Activated	2.00	1.70E-02	
	RARA	ligand-dependent nuclear	Activated	2.24	2.91E-03	
	JNK	group	Inhibited	-2.28	4.06E-09	24 (16)
	NFκB	complex	Inhibited	-2.18	3.97E-03	23 (9)
	ERK	group	Inhibited	-2.93	9.55E-08	30 (16)
	RICTOR	other	Inhibited	-2.34	1.61E-09	
	CCND1	transcription regulator	Inhibited	-2.00	1.50E-02	
	GPER1	g-protein coupled receptor	Inhibited	-2.20	6.95E-06	22 (11)
	HIF1A	transcription regulator	Inhibited	-2.22	2.80E-04	19 (8)
	NUPR1	transcription regulator	Inhibited	-2.50	2.94E-06	
	ATM	kinase	Inhibited	-2.18	4.58E-06	24 (13)
	EGFR	kinase	Inhibited	-2.17	6.33E-03	27 (16)
	TNF	cytokine	Inhibited	-2.49	7.28E-04	27 (14)
	CTGF	growth factor	Inhibited	-2.17	3.65E-05	
	TGFB1	growth factor	Inhibited	-3.60	2.18E-07	29 (11)
	RELA	transcription regulator	Inhibited	-2.20	9.71E-05	27 (11)
	FOXO3	transcription regulator	Inhibited	-2.18	1.31E-03	10 (3)
	ERBB2	kinase	Inhibited	-2.83	2.31E-06	19 (4)
	IL1B	cytokine	Inhibited	-2.06	6.78E-05	22 (13)

The 15v2 contrast, although showing the greatest number of DE genes, discovered fewer significant upstream regulators than the 15v21 contrast. Only two upstream regulators showed upregulation: *PRKAA1* and *DUSP1*. *PRKAA1* suppresses *mTOR* (Corominas-Faja et al., 2013), which is involved in the hypoxic cellular response (Wang et al., 2015), inducing a range of responses including cell growth and vascular remodeling under hypoxic conditions. However, differential *mTOR* expression was not indicated in any of the contrasts performed in this study. *DUSP1* is activated by hypoxia and negatively modulates the activity of HIF1A (Liu et al., 2005; Kučera et al., 2017). Thus, in the 15pct treatment, the hypoxic response may be downregulated by the predicted upregulation of *DUSP1* and *PRKAA1* (Table 4). Suppression of the remaining regulatory molecules was predicted, including suppression of the hypoxia-responsive *HIF1A*, *TLR4*, *RICTOR*, *CD38*, *NEDD9*, *IL5*, and *ATF4* genes (Table 4).

Comparison of the 2pct and 21pct treatments produced only three significantly changed upstream regulators, *HIF1α*, *NEDD9*, and *STAT3,* all of which were increased (Table 4). All of these factors are hypoxia-responsive and upregulated under hypoxic conditions (Martin-Rendon et al., 2007; Niu et al., 2008; Iyer et al., 1998), and suggest a typical hypoxic response. Correspondingly, the two networks derived from the DE genes in the 2v21 contrast involve cancer/cellular growth (-log pval of 40) and the inflammatory response/cellular growth (Table 5). As most hypoxia studies are performed on cancer cells under hypoxic conditions to mimic the hypoxic interior microenvironment of a tumor mass, the response of the bronchial epithelium to maintain cellular viability and growth under the hypoxic assay condition appear to activate a similar regulatory network. The predicted involvement of an inflammatory response is in accordance with the induction of a hypoxic response; inflammation is co-activated with hypoxia genes through the activity of *NFκB* (Bartels et al., 2013).

IPA Network analysis identified 11 individual networks scoring above 10 in the 15v2 gene list, involving cellular assembly/organization, cellular movement, cancer, energy production, dermatological diseases, cell cycle, replication, carbohydrate metabolism, cellular growth, respiratory disease, and embryonic development (Table 5), potentially representing an enrichment of growth and cellular mitigation of the mild hypoxia the cells experienced. Six individual networks were identified in the 15v21 DE list, involving cardiovascular disease, cellular movement, cellular assembly and organization, RNA post-transcriptional modification, and connective tissue development/function. The 2v21 comparison yielded only two significant networks involving cancer/cellular development and inflammation.

Table 5

IPA-predicted Molecular Networks Based on Gene Expression Profiles of Microarray Datasets

Analysis	Score (-log pVal)	Focus Molecules	Top Diseases and Functions
15v2	35	22	Cellular Assembly and Organization, Cellular Movement, Cell Morphology
	31	20	Cellular Movement, Cellular Compromise, Glomerular Injury
	29	19	Cancer, Organismal Injury and Abnormalities, Cellular Movement
	24	17	Cancer, Dermatological Diseases and Conditions, Organismal Injury and Abnormalities
	22	16	Energy Production, Nucleic Acid Metabolism, Small Molecule Biochemistry
	22	16	Dermatological Diseases and Conditions, Organismal Injury and Abnormalities, Cancer
	21	15	Cell Cycle, Cellular Growth and Proliferation, DNA Replication, Recombination, and Repair
	21	15	Carbohydrate Metabolism, Energy Production, Molecular Transport
	17	13	Cellular Growth and Proliferation, Developmental Disorder, Hereditary Disorder
	17	13	Respiratory Disease, Cellular Development, Connective Tissue Development and Function
	13	11	Embryonic Development, Organ Development, Organ Morphology
2v21	40	16	Cancer, Cellular Development, Cellular Growth and Proliferation
	12	6	Inflammatory Response, Cellular Movement, Cellular Growth and Proliferation
15v21	30	18	Cardiovascular Disease, Organismal Injury and Abnormalities, Cell Morphology
	28	17	Cardiac Enlargement, Cardiovascular Disease, Cardiovascular System Development and Function
	26	16	Cellular Movement, Cellular Development, Embryonic Development
	24	15	Cellular Assembly and Organization, DNA Replication, Recombination, and Repair, Post-Translational Modification
	20	13	RNA Post-Transcriptional Modification, Cancer, Cell Death and Survival
	18	12	Connective Tissue Development and Function, Lipid Metabolism, Small Molecule Biochemistry

Note. IPA = Ingenuity Pathway Analysis.

The most significant regulator effect networks identified by IPA in the 15v2 and 15v21 treatments demonstrate the widespread genic downregulation of the 15pct treatment concerning both the normoxic 21pct and hypoxic 2pct condition (Figure 9). In the 15v2 contrast (Figure 9A), only one of the four regulated cellular processes, 'consumption of O_2,' is predicted to increase, while the remaining ('cell proliferation of breast cancer cell line,' 'adhesion of tumor cell lines,' and 'development of body trunk') are downregulated. Of the noted health effects, 'edema' is upregulated, while 'cell death,' 'neurological signs,' and 'atherosclerosis' are downregulated. While the implications of the health effect regulation are not clear, the upregulation of 'consumption of O_2' indicates that the cells in the 15v2 contrast may be consuming O_2 by processes outside the classical hypoxic response in the 15pct condition. Further, only four of the predicted molecular interactions are in opposition to the expected expression pattern, as denoted by the yellow lines in Figure 9A, lending confidence to the predicted regulatory network.

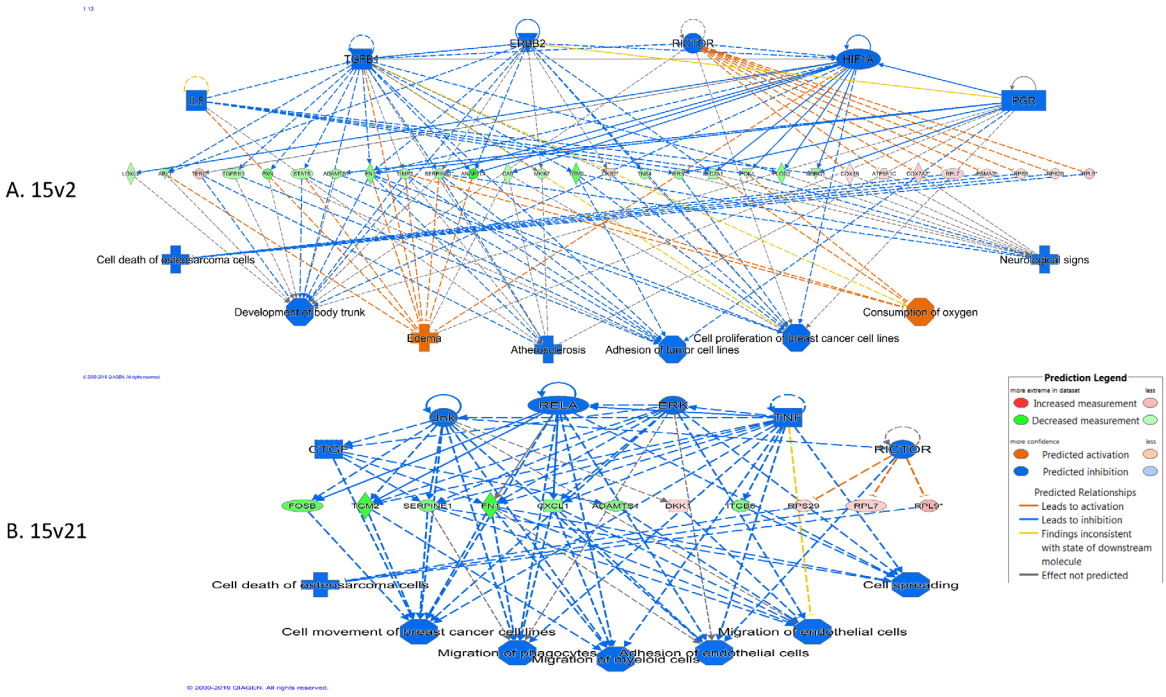


Figure 9. Top predicted regulatory network for each indicated contrast by IPA. A. 15pct vs. 2pct contrast indicates the downregulation of hypoxia regulators and proliferative responses but an increase in edema and oxygen consumption. B. 15pct vs. 21pct contrast indicates a decrease in proliferative functions and cellular activity functions. The key to color-coding is at the bottom right.

In the 15v21 contrast, the top regulatory effect network indicates a global decrease in cellular proliferation and movement, mediated by predicted downregulation of *CTGF*, *JNK*, *RELA*, *ERK*, *TNF*, and *RICTOR* (Table 4). In this predicted network, only one interaction, a suppressive effect of *TNF* on 'Migration of Endothelial Cells,' contravened the predictive matrix (indicated by the

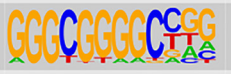
yellow line in Figure 9B). As no regulatory networks were predicted in the 2v21 contrast due to the small number of DE genes, none are shown. The predicted downregulation of upstream effectors *RICTOR*, *TNF*, *ERK*, *RELA*, *JNK*, and *CTGF* was completely consistent with the observed direction-of-expression of measured gene expression. The predicted downregulation of *RELA*, which promotes *NFκB*-mediated transcription (Culver et al., 2010); *RICTOR*, activated during hypoxia (Schmidt et al., 2017); *TNF*, which serves to upregulate inflammatory responses and is activated during hypoxia by *HIF1α* (Ghosh et al., 2013); *ERK*, also activated during hypoxia (Liu et al., 2010); *JNK*, a family of genes upregulated in response to hypoxia with *HIF1α*-inducing activity (Sala et al., 2018); and *CTGF*, a cellular growth factor upregulated by activated *HIF1α* (Higgins et al., 2004), appears to demonstrate the suppression of the *HIF1α*-regulated genes in HBECs exposed to a 15% O_2 environment. Thus, the cellular response to this O_2 level is likely mediated by other avenues, possibly through the large-scale gene upregulation observed here.

The main difference between the 2pct and 21pct treatments was in the upregulation of HIF1α-activated genes and thereby the hypoxic response. The activation of the hypoxic response may have maintained cellular homeostasis, allowing the cells to maintain normal activity while under severe hypoxia, resulting in the similarity in chromatin accessibility and gene expression between the 2pct and 21pct treatments. An alternative hypothesis is that, under the very energetically restrictive 2% O_2 condition, the bronchial epithelial cells used herein suspended the majority of cellular processes to conserve energy and prevent further damage until O_2 was restored. The small number of significant differences between the 2pct and 21pct treatments may signal a global inhibition of the cellular response that serves to inhibit chromatin remodeling. The corresponding small number of DE genes between the 2pct and 21pct treatments may result from global transcriptional repression and preservation of the existing RNA in the still-living cell (Koritzinsky et al., 2006; Staudacher et al., 2015; Batie et al. 2018).

Transcription factor motif analysis

To assess enrichment of transcription factor motifs, we performed de novo motif enrichment analysis on individual consensus narrow peak lists from each treatment with the HOMER software package (findMotifsGenome.pl). The contrasts made were identical to those performed previously. Comparing the 15pct treatment against the 21pct treatment, 36 enriched de novo motifs were discovered with p-values above 1e-50 (Table 6, Supplementary Files 1, 2, and 3). The 15pct vs. 2pct comparison found 26 enriched motifs, and the 2pct vs. 21pct analysis found 28 enriched motifs. Among all enriched motifs (Supplementary Files 1, 2, and 3), only the Nuclear Factor Y motif (*NFY*), a widespread transcription factor responsible for a vast range of cellular functions and responses, including regulatory roles in hypoxia (Ly et al., 2013; Dengler et al., 2013) was enriched in all three comparisons. As two of the comparisons contrast hypoxic states against the normoxic state (15v21, 2v21), and the remaining comparison contrasts two different levels of hypoxia (15v2), *NFY* was likely involved in the hypoxic response only in the 2pct treatment and in other processes in the 15pct and 21pct treatments.

Table 6. Enriched Motifs in Comparison of ATAC-seq Peak Lists of Each Treatment

15v21			15v1			1v21		
TF	Motif	P-val	TF	Motif	P-val	TF	Motif	P-val
Fra1		1e-9533	JunB		1e-12768	JunB		1e-752
ERG		1e-903	ERG		1e-1316	YY1		1e-209
p53		1e-737	BORIS		1e-1147	NFY		1e-166
CEBPB		1e-723	SP2		1e-998	PB0199.1		1e-166
BORIS		1e-639	HLF		1e-746	SP1		1e-153
SP1		1e-502	TEAD3		1e-601	POL006.1		1e-148
TEAD4		1e-381	FOX03		1e-521	ETS		1e-131
FoxJ3		1e-248	RUNX2		1e-365	PB0156.1		1e-124
POL012.1		1e-248	POU4F3		1e-341	CRE		1e-122
RUNX1		1e-232	PB0008.1		1e-340	NRF1		1e-105

Note. ATAC = Assay for Transposase-Accessible Chromatin.

Several motifs were detected in two individual analyses among the top 10 enriched motifs for each contrast. *ERG* and *BORIS* were each enriched in the 15v21 and 15v2 contrasts, suggesting a unique role in response to the 15% O_2 environment. *ERG*, a family of transcription factors activating *HIF1α* expression (Aprelikova et al., 2006) and *BORIS* (synonymous with *CTCFL*), a transcription factor involved in germline cell activation and DNA demethylation (Pugacheva et al., 2015, 2016), perhaps signaling the importance of demethylation in the 15pct treatment in altering the chromatin profile during mild hypoxia, were enriched in the 15v21 and 15v2 comparisons, signaling enrichment in the 15pct treatment. *JunB*, upregulated by hypoxia and activating hypoxia-induced angiogenic pathways (Licht et al., 2006; Schmidt et al., 2007), was enriched in both the 15v2 and 2v21 contrasts. *JunB* enrichment in the 15v2 contrast had the highest significance in the entire set of comparisons (p= $1e10^{-12768}$), reflecting the ability of the mildly hypoxic state to activate the *JunB* transcription factor, whereas the severely hypoxic 2pct state was enriched in *JunB* over the 21pct state in the expression of different *JunB* binding sites. The enrichment of *JunB* in both the 15v2 and 2v21 contrasts may imply that *JunB* enrichment activates differing gene sets in the 15pct and 2pct treatments.

The Unique motifs detected in the 15v21 contrast were *Fra1*, *P53*, *CEBPB*, *TEAD4*, *FOXJ3*, *POL012.1*, and *RUNX1*. *FRA1* has been observed to increase under intermittent hypoxia (Messenger et al., 2012), P53 stabilizes HIF1α and also triggers transcription of cellular stress-response genes during hypoxia and other stresses, although it may also be downregulated by

hypoxia (Sermeus & Michiels, 2011). *CEBPBP* binding has been seen to be downregulated by hypoxia in breast cancer cells in a HIF1α dependent fashion, signifying that alternate mechanisms may be at work in the 15pct treatment (Seifeddine et al., 2008). *TEAD4* plays a role in ROS mitigation (Kaneko & DePamphilis 2013), *FOXJ3* has no known role in hypoxia, but its binding sites may be co-bound by the hypoxia-inducible *FOXO3* (Chen et al., 2016). There is very little available functional information regarding *POL012.1,* and *RUNX1* induces transcription of hematopoietic genes but also inhibits *HIF1α*-mediated transcriptional activation (Peng et al., 2008). Hence, the 15pct treatment does show evidence of hypoxia-induced gene transcription, but the enrichment of *CEBPB*, *TEAD4*, *FOXJ3*, and *RUNX1* suggests that *HIF1α*-mediated responses are not a factor at 15% O_2. Further, *TEAD4*, while not noted to be involved in hypoxia, is known to activate *VEGF* transcription, which is responsible for hypoxia-induced angiogenesis (Teng et al., 2016, Morfoisse et al., 2014).

The unique motifs detected in the 15v2 contrast were *SP2*, *HLF*, *TEAD3*, *FOXO3*, *RUNX2*, *POU4F3*, and *PB0008.1*. *FOXO3* (Bakker et al., 2007), *HLF* (Ema et al., 1999), and *RUNX2* (Lee et al., 2012) all are involved in the hypoxic response and are increased during hypoxia. *RUNX2*, interestingly, serves to stabilize HIF1α protein as well as increase angiogenic responses (Lee et al., 2012). Data on *POU4F3* and *PB0008.1* are insufficient to predict a functional role. Thus, the contrast of the 15pct and 2pct treatment shows an increase in many hypoxic response motifs in the 15pct treatment.

Unique motifs in the 2v21 contrast were *YY1*, *PB0199.1*, *POL006.1*, *ETS*, *PB0156.1*, *CRE*, and *NRF1*. *YY1* (Wu et al., 2012), *ETS* (Aprelikova et al., 2006), *CRE* (Taylor et al., 2000), and *NRF1* (Chepelev et al., 2011) are activated during hypoxia, and play roles focused on HIF1α stabilization, although *NRF1* has also been shown to inhibit *HIF1α* (Wang et al., 2016). No published data are available for the transcription factors *PB0199.1*, *Pol006.1*, or *PB0156.1*. The transcription factor profile of the 2pct treatment in contrast to the 21pct treatment revealed a largely hypoxic response, as expected. To test the accuracy of these motif analyses, the reciprocal analyses were performed (21v1, 21v15, and 1v15, data not shown); each reciprocal motif analysis produced substantially different results. The additional *JunB* binding sites expressed in the 15pct treatment were not sufficient to reach significance, yet the additional *JunB* binding sites found in 2pct treatment are even more significantly different from the 15pct treatment.

Conclusions

This study demonstrated that a mildly hypoxic environment simulating the atmospheric composition of a pressurized aircraft cabin at cruising altitude (15% O_2) causes significant changes in both the gene expression profile and chromatin accessibility of cultured HBECs. We also demonstrated a relative lack of alterations in chromatin accessibility or large-scale changes in gene expression, centering on a hypoxia response, within cultured HBECs under the hypoxic state of 2% O_2, an O_2 level used in many cancer studies and which simulates the O_2-poor intra-tumor environment encountered by many cells enclosed within solid tumors. The substantial

response at 15% O_2 may have been due to a cellular attempt to mitigate and overcome this mild reduction in O_2 levels. In comparison, the relative lack of response at 2% O_2 may have been attributable to a global suspension of cellular and transcriptional activity at this unusually low O_2 level. To confirm and better address the findings of this study, an expanded research protocol is necessary, with 1) additional individual subjects represented among the population assayed, 2) increased read depth in the ATAC-seq portion of the study, preferably surpassing 100 million filtered reads per replicate, and 3) similar use of microarrays or RNAseq-based gene expression analysis to capture concurrent gene expression data.

Supplementary Tables, Figures, and Files.

Supplementary Table 1. Combined (union) list of called ATAC-seq peaks for all treatments.

Supplementary Table 2. Feature counts table of reads mapping to each called ATAC-seq peak in the union peak list.

Supplementary Table 3. Differentially expressed ATAC-seq peaks in 15pct vs. 21pct treatments.

Supplementary Table 4. Differentially expressed ATAC-seq peaks in 15pct vs. 2pct treatments.

Supplementary Table 5. Differentially Expressed ATAC-seq peaks in 2pct vs. 21pct treatments.

Supplementary Table 6. Differentially expressed transcript clusters in microarray comparison of 15pct vs. 21pct treatments.

Supplementary Table 7. Differentially expressed transcript clusters in microarray comparison of 15pct vs. 2pct treatments.

Supplementary Table 8. Differentially expressed transcript clusters in microarray comparison of 2pct vs. 21pct treatments.

Supplementary Table 9. Intersection of DE ATAC peaks and DE microarray-identified genes in the 2pct vs. 21pct comparison.

Supplementary Table 10. Intersection of DE ATAC peaks and DE microarray-identified genes in the 15pct vs. 21pct comparison.

Supplementary Table 11. Intersection of DE ATAC peaks and DE microarray-identified genes in the 15pct vs. 2pct comparison.

Supplementary File 1. Differential motif analysis of ATAC-seq peaks called in 15pct vs. 21pct contrast. Enriched motifs are more highly represented in 15pct peak list.

Supplementary File 2. Differential motif analysis of ATAC-seq peaks called in 15pct vs. 2pct contrast. Enriched motifs are more highly represented in 15pct peak list.

Supplementary File 3. Differential motif analysis of ATAC-seq peaks called in 2pct vs. 21pct contrast. Enriched motifs are more highly represented in 2pct peak list.

References

Aprelikova, O., Wood, M., Tackett, S., Chandramouli, G. V., & Barrett, J. C. (2006). Role of ETS transcription factors in the hypoxia-inducible factor-2 target gene selection. *Cancer Research*, *66*(11), 5641–5647. https://doi.org/10.1158/0008-5472.CAN-05-3345.

Bakker, W. J., Harris, I. S., & Mak, T. W. (2007). FOXO3a is activated in response to hypoxic stress and inhibits HIF1-induced apoptosis via regulation of CITED2. *Molecular Cell*, *28*(6), 941–953. https://doi.org/10.1016/j.molcel.2007.10.035.

Batie, M., Del Peso, L., & Rocha, S. (2018). Hypoxia and Chromatin: A Focus on Transcriptional Repression Mechanisms. *Biomedicines, 6*(2), 47. https://doi.org/10.3390/biomedicines6020047

Bartels, K., Grenz, A., & Eltzschig, H. K. (2013). Hypoxia and inflammation are two sides of the same coin. *Proceedings of the National Academy of Sciences of the United States of America, 110*(46), 18351–18352. https://doi.org/10.1073/pnas.1318345110

Baze, M. M., Schlauch, K., & Hayes, J. P. (2010). Gene expression of the liver in response to chronic hypoxia. *Physiological Genomics, 41*(3), 275–288. https://doi.org/10.1152/physiolgenomics.00075.2009

Belaiba, R. S., Bonello, S., Zähringer, C., Schmidt, S., Hess, J., Kietzmann, T., & Görlach, A. (2007). Hypoxia upregulates hypoxia-inducible factor-1alpha transcription by involving phosphatidylinositol 3-kinase and nuclear factor kappaB in pulmonary artery smooth muscle cells. *Molecular Biology of the Cell, 18*(12), 4691–4697. https://doi.org/10.1091/mbc.e07-04-0391

Buenrostro, J. D., Wu, B., Chang, H. Y., & Greenleaf, W. J. (2015). ATAC-seq: A Method for Assaying Chromatin Accessibility Genome-Wide. *Current Protocols in Molecular Biology, 109*, 21.29.1–21.29.9. https://doi.org/10.1002/0471142727.mb2129s109

Burki, N. K., & Tetenta, S. U. (2014). Inflammatory response to acute hypoxia in humans. *Pulmonary Pharmacology & Therapeutics, 27*(2), 208–211. https://doi.org/10.1016/j.pupt.2013.05.008

Chen, X., Ji, Z., Webber, A., & Sharrocks, A. D. (2016). Genome-wide binding studies reveal DNA binding specificity mechanisms and functional interplay amongst Forkhead transcription factors. *Nucleic Acids Research, 44*(4), 1566–1578. https://doi.org/10.1093/nar/gkv1120

Cheng, G., Zhong, M., Kawaguchi, R., Kassai, M., Al-Ubaidi, M., Deng, J., Ter-Stepanian, M., & Sun, H. (2014). Identification of PLXDC1 and PLXDC2 as the transmembrane receptors for the multifunctional factor PEDF. *eLife, 3*, e05401. https://doi.org/10.7554/eLife.05401

Chepelev, N. L., Bennitz, J. D., Huang, T., McBride, S., & Willmore, W. G. (2011). The Nrf1 CNC-bZIP protein is regulated by the proteasome and activated by hypoxia. *PloS One, 6*(12), e29167. https://doi.org/10.1371/journal.pone.0029167

Corces, M. R., Trevino, A. E., Hamilton, E. G., Greenside, P. G., Sinnott-Armstrong, N. A., Vesuna, S., Satpathy, A. T., Rubin, A. J., Montine, K. S., Wu, B., Kathiria, A., Cho, S. W., Mumbach, M. R., Carter, A. C., Kasowski, M., Orloff, L. A., Risca, V. I., Kundaje, A., Khavari, P. A., Montine, T. J., … Chang, H. Y. (2017). An improved ATAC-seq protocol reduces background and enables interrogation of frozen tissues. *Nature Methods, 14*(10), 959–962. https://doi.org/10.1038/nmeth.4396

Corominas-Faja, B., Cufí, S., Oliveras-Ferraros, C., Cuyàs, E., López-Bonet, E., Lupu, R., Alarcón, T., Vellon, L., Iglesias, J. M., Leis, O., Martín, Á. G., Vazquez-Martin, A., & Menendez, J. A. (2013). Nuclear reprogramming of luminal-like breast cancer cells generates Sox2-overexpressing cancer stem-like cellular states harboring transcriptional activation of the mTOR pathway. *Cell Cycle (Georgetown, Tex.), 12*(18), 3109–3124. https://doi.org/10.4161/cc.26173

Culver, C., Sundqvist, A., Mudie, S., Melvin, A., Xirodimas, D., & Rocha, S. (2010). Mechanism of hypoxia-induced NF-kappaB. *Molecular and Cellular Biology, 30*(20), 4901–4921. https://doi.org/10.1128/MCB.00409-10

Dengler, V. L., Galbraith, M., & Espinosa, J. M. (2014). Transcriptional regulation by hypoxia inducible factors. *Critical Reviews in Biochemistry and Molecular Biology, 49*(1), 1–15. https://doi.org/10.3109/10409238.2013.838205

Ema, M., Hirota, K., Mimura, J., Abe, H., Yodoi, J., Sogawa, K., Poellinger, L., & Fujii-Kuriyama, Y. (1999). Molecular mechanisms of transcription activation by HLF and HIF1alpha in response to hypoxia: their stabilization and redox signal-induced interaction with CBP/p300. *The EMBO Journal, 18*(7), 1905–1914. https://doi.org/10.1093/emboj/18.7.1905

Ghosh, S., Paul, A., & Sen, E. (2013). Tumor necrosis factor α-induced hypoxia-inducible factor 1α-β-catenin axis regulates major histocompatibility complex class I gene activation through chromatin remodeling. *Molecular and Cellular Biology, 33*(14), 2718–2731. https://doi.org/10.1128/MCB.01254-12

Gusarova, V., O'Dushlaine, C., Teslovich, T. M., Benotti, P. N., Mirshahi, T., Gottesman, O., Van Hout, C. V., Murray, M. F., Mahajan, A., Nielsen, J. B., Fritsche, L., Wulff, A. B., Gudbjartsson, D. F., Sjögren, M., Emdin, C. A., Scott, R. A., Lee, W. J., Small, A., Kwee, L. C., Dwivedi, O. P., … Gromada, J. (2018). Genetic inactivation of ANGPTL4 improves glucose homeostasis and is associated with reduced risk of diabetes. *Nature Communications, 9*(1), 2252. https://doi.org/10.1038/s41467-018-04611-z

Gustafsson, M. V., Zheng, X., Pereira, T., Gradin, K., Jin, S., Lundkvist, J., Ruas, J. L., Poellinger, L., Lendahl, U., & Bondesson, M. (2005). Hypoxia requires notch signaling to maintain the

undifferentiated cell state. *Developmental Cell*, *9*(5), 617–628. https://doi.org/10.1016/j.devcel.2005.09.010

Heinz, S., Benner, C., Spann, N., Bertolino, E., Lin, Y. C., Laslo, P., Cheng, J. X., Murre, C., Singh, H., & Glass, C. K. (2010). Simple combinations of lineage-determining transcription factors prime cis-regulatory elements required for macrophage and B cell identities. *Molecular Cell, 38*(4), 576–589. https://doi.org/10.1016/j.molcel.2010.05.004

Higgins, D. F., Biju, M. P., Akai, Y., Wutz, A., Johnson, R. S., & Haase, V. H. (2004). Hypoxic induction of Ctgf is directly mediated by Hif-1. *American Journal of Physiology. Renal Physiology, 287*(6), F1223–F1232. https://doi.org/10.1152/ajprenal.00245.2004

Iyer, N. V., Leung, S. W., & Semenza, G. L. (1998). The human hypoxia-inducible factor 1alpha gene: HIF1A structure and evolutionary conservation. *Genomics, 52*(2), 159–165. https://doi.org/10.1006/geno.1998.5416

Kaneko, K. J., & DePamphilis, M. L. (2013). TEAD4 establishes the energy homeostasis essential for blastocoel formation. *Development (Cambridge, England), 140*(17), 3680–3690. https://doi.org/10.1242/dev.093799

Kaur, A., Van, P. T., Busch, C. R., Robinson, C. K., Pan, M., Pang, W. L., Reiss, D. J., DiRuggiero, J., & Baliga, N. S. (2010). Coordination of frontline defense mechanisms under severe oxidative stress. *Molecular Systems Biology, 6*, 393. https://doi.org/10.1038/msb.2010.50

Koritzinsky, M., Magagnin, M. G., van den Beucken, T., Seigneuric, R., Savelkouls, K., Dostie, J., Pyronnet, S., Kaufman, R. J., Weppler, S. A., Voncken, J. W., Lambin, P., Koumenis, C., Sonenberg, N., & Wouters, B. G. (2006). Gene expression during acute and prolonged hypoxia is regulated by distinct mechanisms of translational control. *The EMBO Journal, 25*(5), 1114–1125. https://doi.org/10.1038/sj.emboj.7600998

Kučera, J., Netušilová, J., Sladeček, S., Lánová, M., Vašíček, O., Štefková, K., Navrátilová, J., Kubala, L., & Pacherník, J. (2017). Hypoxia Downregulates MAPK/ERK but Not STAT3 Signaling in ROS-Dependent and HIF-1-Independent Manners in Mouse Embryonic Stem Cells. *Oxidative Medicine and Cellular Longevity, 2017*, 4386947.

Kunjade, A. (2020). kundajelab/cut-n-run-pipeline. GitHub. https://github.com/kundajelab/atac-seq-pipeline

Lee, J. W., Yang, D. H., Park, S., Han, H. K., Park, J. W., Kim, B. Y., Um, S. H., & Moon, E. Y. (2017). Trichostatin A resistance is facilitated by HIF-1α acetylation in HeLa human cervical cancer cells under normoxic conditions. *Oncotarget, 9*(2), 2035–2049. https://doi.org/10.18632/oncotarget.23327

Lee, S. H., Che, X., Jeong, J. H., Choi, J. Y., Lee, Y. J., Lee, Y. H., Bae, S. C., & Lee, Y. M. (2012). Runx2 protein stabilizes hypoxia-inducible factor-1α through competition with von Hippel-Lindau protein (pVHL) and stimulates angiogenesis in growth plate hypertrophic chondrocytes. *The Journal of Biological Chemistry, 287*(18), 14760–14771.

Li, Y. Y., Chung, G. T., Lui, V. W., To, K. F., Ma, B. B., Chow, C., Woo, J. K., Yip, K. Y., Seo, J., Hui, E. P., Mak, M. K., Rusan, M., Chau, N. G., Or, Y. Y., Law, M. H., Law, P. P., Liu, Z. W., Ngan, H. L., Hau, P. M., Verhoeft, K. R., … Lo, K. W. (2017). Exome and genome sequencing of nasopharynx cancer identifies NF-κB pathway activating mutations. *Nature Communications, 8*, 14121. https://doi.org/10.1038/ncomms14121

Liao, Y., Smyth, G. K., & Shi, W. (2013). The Subread aligner: fast, accurate and scalable read mapping by seed-and-vote. *Nucleic Acids Research, 41*(10), e108. https://doi.org/10.1093/nar/gkt214

Liao, Y., Smyth, G. K., & Shi, W. (2014). featureCounts: an efficient general purpose program for assigning sequence reads to genomic features. *Bioinformatics (Oxford, England), 30*(7), 923–930. https://doi.org/10.1093/bioinformatics/btt656

Licht, A. H., Pein, O. T., Florin, L., Hartenstein, B., Reuter, H., Arnold, B., Lichter, P., Angel, P., & Schorpp-Kistner, M. (2006). JunB is required for endothelial cell morphogenesis by regulating core-binding factor beta. *The Journal of Cell Biology, 175*(6), 981–991.

Liu, C., Shi, Y., Du, Y., Ning, X., Liu, N., Huang, D., Liang, J., Xue, Y., & Fan, D. (2005). Dual-specificity phosphatase DUSP1 protects overactivation of hypoxia-inducible factor 1 through inactivating ERK MAPK. *Experimental Cell Research, 309*(2), 410–418. https://doi.org/10.1016/j.yexcr.2005.06.022

Liu, L., Zhang, H., Sun, L., Gao, Y., Jin, H., Liang, S., Wang, Y., Dong, M., Shi, Y., Li, Z., & Fan, D. (2010). ERK/MAPK activation involves hypoxia-induced MGr1-Ag/37LRP expression and contributes to apoptosis resistance in gastric cancer. *International Journal of Cancer, 127*(4), 820–829. https://doi.org/10.1002/ijc.25098

Ly, L. L., Yoshida, H., & Yamaguchi, M. (2013). Nuclear transcription factor Y and its roles in cellular processes related to human disease. *American Journal of Cancer Research, 3*(4), 339–346.

Majmundar, A. J., Wong, W. J., & Simon, M. C. (2010). Hypoxia-inducible factors and the response to hypoxic stress. *Molecular Cell, 40*(2), 294–309. https://doi.org/10.1016/j.molcel.2010.09.022

Martin-Rendon, E., Hale, S. J., Ryan, D., Baban, D., Forde, S. P., Roubelakis, M., Sweeney, D., Moukayed, M., Harris, A. L., Davies, K., & Watt, S. M. (2007). Transcriptional profiling of human cord blood CD133+ and cultured bone marrow mesenchymal stem cells in response to hypoxia. *Stem Cells (Dayton, Ohio), 25*(4), 1003–1012. https://doi.org/10.1634/stemcells.2006-0398

McCarthy, D. J., Chen, Y., & Smyth, G. K. (2012). Differential expression analysis of multifactor RNA-Seq experiments with respect to biological variation. *Nucleic Acids Research, 40*(10), 4288–4297. https://doi.org/10.1093/nar/gks042

Melvin, A., & Rocha, S. (2012). Chromatin as an oxygen sensor and active player in the hypoxia response. *Cellular Signalling, 24*(1), 35–43. https://doi.org/10.1016/j.cellsig.2011.08.019

Messenger, S. A., Moreau, J. M., & Ciriello, J. (2012). Intermittent hypoxia and systemic leptin administration induces pSTAT3 and Fos/Fra-1 in the carotid body. *Brain Research, 1446*, 56–70. https://doi.org/10.1016/j.brainres.2012.01.074

Mimura, I., Nangaku, M., Kanki, Y., Tsutsumi, S., Inoue, T., Kohro, T., Yamamoto, S., Fujita, T., Shimamura, T., Suehiro, J., Taguchi, A., Kobayashi, M., Tanimura, K., Inagaki, T., Tanaka, T., Hamakubo, T., Sakai, J., Aburatani, H., Kodama, T., & Wada, Y. (2012). Dynamic change of chromatin conformation in response to hypoxia enhances the expression of GLUT3 (SLC2A3) by cooperative interaction of hypoxia-inducible factor 1 and KDM3A. *Molecular and Cellular Biology, 32*(15), 3018–3032.

Morfoisse, F., Kuchnio, A., Frainay, C., Gomez-Brouchet, A., Delisle, M. B., Marzi, S., Helfer, A-C., Hantelys, F., Pujol, F., Guillermet-Guibert, J., Bousquet, C., Dewerchin, M., Pyronnet, S., Prats, A-C., Carmeliet, P., & Garmy-Susini, B. (2014). Hypoxia induces VEGF-C expression in metastatic tumor cells via a HIF-1α-independent translation-mediated mechanism. *Cell reports*, *6*(1), 155-167.

Muhm, J. M., Rock, P. B., McMullin, D. L., Jones, S. P., Lu, I. L., Eilers, K. D., Space, D. R., & McMullen, A. (2007). Effect of aircraft-cabin altitude on passenger discomfort. *The New England Journal of Medicine, 357*(1), 18–27. https://doi.org/10.1056/NEJMoa062770

Muth, M., Hussein, K., Jacobi, C., Kreipe, H., & Bock, O. (2011). Hypoxia-induced down-regulation of microRNA-449a/b impairs control over targeted SERPINE1 (PAI-1) mRNA - a mechanism involved in SERPINE1 (PAI-1) overexpression. *Journal of Translational Medicine, 9*, 24.

National Center for Biotechnology Information. (n.d.). *NCBI Genome Remapping Service*. Retrieved September 14, 2020, from https://www.ncbi.nlm.nih.gov/genome/tools/remap

Neph, S., Kuehn, M. S., Reynolds, A. P., Haugen, E., Thurman, R. E., Johnson, A. K., Rynes, E., Maurano, M. T., Vierstra, J., Thomas, S., Sandstrom, R., Humbert, R., & Stamatoyannopoulos, J. A. (2012). BEDOPS: high-performance genomic feature operations. *Bioinformatics (Oxford, England), 28*(14), 1919–1920. https://doi.org/10.1093/bioinformatics/bts277

Niu, G., Briggs, J., Deng, J., Ma, Y., Lee, H., Kortylewski, M., Kujawski, M., Kay, H., Cress, W. D., Jove, R., & Yu, H. (2008). Signal transducer and activator of transcription 3 is required for hypoxia-inducible factor-1alpha RNA expression in both tumor cells and tumor-associated myeloid cells. *Molecular Cancer Research : MCR, 6*(7), 1099–1105. https://doi.org/10.1158/1541-7786.MCR-07-2177

Olcina, M. M., Grand, R. J., & Hammond, E. M. (2014). ATM activation in hypoxia - causes and consequences. *Molecular & Cellular Oncology, 1*(1), e29903. https://doi.org/10.4161/mco.29903

Ortiz-Barahona, A., Villar, D., Pescador, N., Amigo, J., & del Peso, L. (2010). Genome-wide identification of hypoxia-inducible factor binding sites and target genes by a probabilistic model integrating transcription-profiling data and in silico binding site prediction. *Nucleic Acids Research, 38*(7), 2332–2345. https://doi.org/10.1093/nar/gkp1205

Peacock A. J. (1998). ABC of oxygen: oxygen at high altitude. *BMJ (Clinical Research Ed.), 317*(7165), 1063–1066. https://doi.org/10.1136/bmj.317.7165.1063

Peng, Z. G., Zhou, M. Y., Huang, Y., Qiu, J. H., Wang, L. S., Liao, S. H., Dong, S., & Chen, G. Q. (2008). Physical and functional interaction of Runt-related protein 1 with hypoxia-inducible factor-1alpha. *Oncogene, 27*(6), 839–847.

Pressurized Cabins, 45 C.F.R § 25.841 (2012). https://www.govinfo.gov/app/details/CFR-2012-title14-vol1/CFR-2012-title14-vol1-sec25-841

Prickaerts, P., Adriaens, M. E., Beucken, T., Koch, E., Dubois, L., Dahlmans, V., Gits, C., Evelo, C., Chan-Seng-Yue, M., Wouters, B. G., & Voncken, J. W. (2016). Hypoxia increases genome-wide bivalent epigenetic marking by specific gain of H3K27me3. *Epigenetics & Chromatin, 9*, 46. https://doi.org/10.1186/s13072-016-0086-0

Pugacheva, E. M., Rivero-Hinojosa, S., Espinoza, C. A., Méndez-Catalá, C. F., Kang, S., Suzuki, T., Kosaka-Suzuki, N., Robinson, S., Nagarajan, V., Ye, Z., Boukaba, A., Rasko, J. E., Strunnikov, A. V., Loukinov, D., Ren, B., & Lobanenkov, V. V. (2015). Comparative analyses of CTCF and BORIS occupancies uncover two distinct classes of CTCF binding genomic regions. *Genome Biology, 16*(1), 161. https://doi.org/10.1186/s13059-015-0736-8

Pugacheva, E. M., Teplyakov, E., Wu, Q., Li, J., Chen, C., Meng, C., Liu, J., Robinson, S., Loukinov, D., Boukaba, A., Hutchins, A. P., Lobanenkov, V., & Strunnikov, A. (2016). The cancer-associated CTCFL/BORIS protein targets multiple classes of genomic repeats, with a distinct binding and functional preference for humanoid-specific SVA transposable elements. *Epigenetics & Chromatin, 9*(1), 35. https://doi.org/10.1186/s13072-016-0084-2

Quinlan A. R. (2014). BEDTools: The Swiss-Army Tool for Genome Feature Analysis. *Current Protocols in Bioinformatics, 47*, 11.12.1–11.12.34. https://doi.org/10.1002/0471250953.bi1112s47

Ramírez, F., Dündar, F., Diehl, S., Grüning, B. A., & Manke, T. (2014). deepTools: a flexible platform for exploring deep-sequencing data. *Nucleic Acids Research, 42*(Web Server issue), W187–W191. https://doi.org/10.1093/nar/gku365

Rao, N. A., McCalman, M. T., Moulos, P., Francoijs, K. J., Chatziioannou, A., Kolisis, F. N., Alexis, M. N., Mitsiou, D. J., & Stunnenberg, H. G. (2011). Coactivation of GR and NFKB alters the repertoire of their binding sites and target genes. *Genome Research, 21*(9), 1404–1416.

Ritchie, M. E., Phipson, B., Wu, D., Hu, Y., Law, C. W., Shi, W., & Smyth, G.K. (2015) limma powers differential expression analyses for RNA-sequencing and microarray studies. *Nucleic Acids Research* 43(7): e47

Roach, R. C., Hackett, P. H., Oelz, O., Bärtsch, P., Luks, A. M., MacInnis, M. J., Baillie, J. K., & Lake Louise AMS Score Consensus Committee (2018). The 2018 Lake Louise Acute Mountain Sickness Score. *High Altitude Medicine & Biology, 19*(1), 4–6. https://doi.org/10.1089/ham.2017.0164

Robinson, J. T., Thorvaldsdóttir, H., Winckler, W., Guttman, M., Lander, E. S., Getz, G., & Mesirov, J. P. (2011). Integrative genomics viewer. *Nature Biotechnology, 29*(1), 24–26. https://doi.org/10.1038/nbt.1754

Robinson, M. D., McCarthy, D. J., & Smyth, G. K. (2010). edgeR: a Bioconductor package for differential expression analysis of digital gene expression data. *Bioinformatics (Oxford, England), 26*(1), 139–140. https://doi.org/10.1093/bioinformatics/btp616

Sala, M. A., Chen, C., Zhang, Q., Do-Umehara, H. C., Wu, W., Misharin, A. V., Waypa, G. B., Fang, D., Budinger, G., Liu, S., Chandel, N. S., Schumacker, P. T., Sznajder, J. I., & Liu, J. (2018). JNK2 upregulates hypoxia-inducible factors and contributes to hypoxia-induced erythropoiesis and pulmonary hypertension. *The Journal of Biological Chemistry, 293*(1), 271–284. https://doi.org/10.1074/jbc.RA117.000440

Sarkar, S., Banerjee, P. K., & Selvamurthy, W. (2003). High altitude hypoxia: an intricate interplay of oxygen responsive macroevents and micromolecules. *Molecular and Cellular Biochemistry, 253*(1-2), 287–305. https://doi.org/10.1023/a:1026080320034

Schmidt, D., Textor, B., Pein, O. T., Licht, A. H., Andrecht, S., Sator-Schmitt, M., Fusenig, N. E., Angel, P., & Schorpp-Kistner, M. (2007). Critical role for NF-kappaB-induced JunB in VEGF regulation and tumor angiogenesis. *The EMBO Journal, 26*(3), 710–719. https://doi.org/10.1038/sj.emboj.7601539

Schmidt, K. M., Hellerbrand, C., Ruemmele, P., Michalski, C. W., Kong, B., Kroemer, A., Hackl, C., Schlitt, H. J., Geissler, E. K., & Lang, S. A. (2017). Inhibition of mTORC2 component RICTOR impairs tumor growth in pancreatic cancer models. *Oncotarget, 8*(15), 24491–24505. https://doi.org/10.18632/oncotarget.15524

Seifeddine, R., Dreiem, A., Blanc, E., Fulchignoni-Lataud, M. C., Le Frère Belda, M. A., Lecuru, F., Mayi, T. H., Mazure, N., Favaudon, V., Massaad, C., Barouki, R., & Massaad-Massade, L. (2008). Hypoxia down-regulates CCAAT/enhancer binding protein-alpha expression in breast cancer cells. *Cancer Research, 68*(7), 2158–2165. https://doi.org/10.1158/0008-5472.CAN-07-1190

Semenza, G. L., Agani, F., Booth, G., Forsythe, J., Iyer, N., Jiang, B. H., Leung, S., Roe, R., Wiener, C., & Yu, A. (1997). Structural and functional analysis of hypoxia-inducible factor 1. *Kidney International, 51*(2), 553–555. https://doi.org/10.1038/ki.1997.77

Sermeus, A., & Michiels, C. (2011). Reciprocal influence of the p53 and the hypoxic pathways. *Cell Death & Disease, 2*(5), e164. https://doi.org/10.1038/cddis.2011.48

Srinivasan, S., Chitalia, V., Meyer, R. D., Hartsough, E., Mehta, M., Harrold, I., Anderson, N., Feng, H., Smith, L. E., Jiang, Y., Costello, C. E., & Rahimi, N. (2015). Hypoxia-induced expression of phosducin-like 3 regulates expression of VEGFR-2 and promotes angiogenesis. *Angiogenesis, 18*(4), 449–462. https://doi.org/10.1007/s10456-015-9468-3

Staudacher, J. J., Naarmann-de Vries, I. S., Ujvari, S. J., Klinger, B., Kasim, M., Benko, E., Ostareck-Lederer, A., Ostareck, D. H., Bondke Persson, A., Lorenzen, S., Meier, J. C., Blüthgen, N., Persson, P. B., Henrion-Caude, A., Mrowka, R., & Fähling, M. (2015). Hypoxia-induced gene expression results from selective mRNA partitioning to the endoplasmic reticulum. *Nucleic Acids Research, 43*(6), 3219–3236. https://doi.org/10.1093/nar/gkv167

Taylor, C. T., Furuta, G. T., Synnestvedt, K., & Colgan, S. P. (2000). Phosphorylation-dependent targeting of cAMP response element binding protein to the ubiquitin/proteasome pathway in hypoxia. *Proceedings of the National Academy of Sciences*, *97*(22), 12091-12096.

Teng, K., Deng, C., Xu, J., Men, Q., Lei, T., Di, D., Liu, T., Li, W., & Liu, X. (2016). Nuclear localization of TEF3-1 promotes cell cycle progression and angiogenesis in cancer. *Oncotarget, 7*(12), 13827–13841. https://doi.org/10.18632/oncotarget.7342

Thorvaldsdóttir, H., Robinson, J. T., & Mesirov, J. P. (2013). Integrative Genomics Viewer (IGV): high-performance genomics data visualization and exploration. *Briefings in Bioinformatics, 14*(2), 178–192. https://doi.org/10.1093/bib/bbs017

Tiede, L. M., Cook, E. A., Morsey, B., & Fox, H. S. (2011). Oxygen matters: tissue culture oxygen levels affect mitochondrial function and structure as well as responses to HIV viroproteins. *Cell Death & Disease, 2*(12), e246. https://doi.org/10.1038/cddis.2011.128

Wang, A. P., Li, X. H., Yang, Y. M., Li, W. Q., Zhang, W., Hu, C. P., Zhang, Z., & Li, Y. J. (2015). A Critical Role of the mTOR/eIF2α Pathway in Hypoxia-Induced Pulmonary Hypertension. *PloS One, 10*(6), e0130806. https://doi.org/10.1371/journal.pone.0130806

Wang, D., Zhang, J., Lu, Y., Luo, Q., & Zhu, L. (2016). Nuclear respiratory factor-1 (NRF-1) regulated hypoxia-inducible factor-1α (HIF-1α) under hypoxia in HEK293T. *IUBMB Life, 68*(9), 748–755. https://doi.org/10.1002/iub.1537

Wu, W., Dave, N. B., Yu, G., Strollo, P. J., Kovkarova-Naumovski, E., Ryter, S. W., Reeves, S. R., Dayyat, E., Wang, Y., Choi, A. M., Gozal, D., & Kaminski, N. (2008). Network analysis of

temporal effects of intermittent and sustained hypoxia on rat lungs. *Physiological Genomics, 36*(1), 24–34. https://doi.org/10.1152/physiolgenomics.00258.2007

Wu, T. Y., Ding, S. Q., Liu, J. L., Jia, J. H., Chai, Z. C., Dai, R. C., Zhao, J. Z., Tang, Q. D., & Kayser, B. (2012). Smoking, acute mountain sickness and altitude acclimatisation: a cohort study. *Thorax, 67*(10), 914–919. https://doi.org/10.1136/thoraxjnl-2011-200623

Yen, K., Lee, C., Mehta, H., & Cohen, P. (2013). The emerging role of the mitochondrial-derived peptide humanin in stress resistance. *Journal of Molecular Endocrinology, 50*(1), R11–R19. https://doi.org/10.1530/JME-12-0203